Journal of Inorganic and General Chemistry
ZAAC
Zeitschrift für anorganische und allgemeine Chemie
www.zaac.wiley-vch.de
RESEARCH ARTICLE
DOI: 10.1002/zaac.202200199

Synthesis and crystal structures of rhodium acetate paddle-wheel complexes with anchor group-functionalised and hydrogen bond-supported axial ligands

André Mang,[a] Michael Linseis,[a] and Rainer F. Winter*[a]

Dedicated to Prof. Dr. Thomas Schleid on the occasion of his 65th birthday with personal thanks of RFW for introducing him to the world of Islays.

We report the synthesis and X-ray structures of four $Rh_2(OAc)_4(L_{Ax})_2$ (OAc = acetate, CH_3COO^-) paddle-wheel complexes (**C1**–**C4**) with methylthio-modified axial ligands L_{Ax} derived from benzamidine (**L1**), anilinopyrimidine (**L2**) or isothiourea (**L3**, **L4**) that are capable of forming N–H···O hydrogen bonds to the equatorially bridging acetate ligands. This was done with the aim to suppress dissociation of the axial ligands and to make the complexes amenable to single-molecule conductance measurements in a scanning tunneling microscope break-junction (STM-BJ) setup. The characteristic spectroscopic features (NMR, IR, vis), crystal structures, the hydrogen-bonding motifs and a DFT-based screening of their frontier molecular orbitals are presented. Our calculations suggest that hydrogen-bonding stabilises axial ligand binding by 15 kJ/mol to 30 kJ/mol and that the HOMO of the rhodium paddle-wheels is closer to the Au work function than the LUMO, so that the rhodium paddle-wheels are expected to constitute hole conductors.

Introduction

Ever since the discovery of direct metal-metal (M–M) bonding in dinuclear acetato complexes of chromium,[1] the resulting so-called paddle-wheel or Chinese lantern motifs drew tremendous attention of the scientific community. In this structural archetype, two transition metal ions are held in close spatial proximity *via* four laterally (equatorially) attached, bridging carboxylate ligands. Their close approach allows for efficient d-orbital overlap with concomitant formation of direct metal-metal bonds as a key feature. Depending on the electronic configuration of the metal ions, bond orders ranging from zero (d^8) to up to four (d^4) can be realised in such architectures, which is duly reflected in the M–M distances (Scheme 1). Particularly spectacular were the metal-metal quadruple bonds in chromium(II) and molybdenum(II) acetate (d_{Cr-Cr} = 2.362(1) Å,[2] d_{Mo-Mo} = 2.110(3) Å[3]), while their structural congener rhodium(II) acetate (d_{Rh-Rh} = 2.386(3) Å)[2] with its d^7 electron count only exhibits a Rh–Rh single bond (panel B, Scheme 1).[4]

Besides carboxylates (cbs'),[5] a variety of other bridging, bidentate chelate ligands such as formamidinates (fas')[6] benzamidinates (bas')[7] or anilinopyridinates (aps')[8] with π-conjugated aromatic backbones may serve as the equatorial clamping ligands in paddle-wheel complexes. The asset of tunable metal-metal bond order and the prospect of introducing further functionalities through the bridging or axially coordinated ligands L_{Ax} (Scheme 1, panel A) render the paddle-wheel scaffold a versatile structural template for further exploitation. Appropriately designed paddle-wheel complexes have found use as molecular building blocks for the assembly of supramolecular macrostructures and chainlike arrays,[6b,9] mainly through the selective capping and linking approach of Cotton *et al.*[6b] This approach draws on the selective formation of *cis*- or *trans*-configured heteroleptic paddle-wheel complexes with two different kinds of equatorial bridging ligands from their homoleptic precursors. As an example, selective *trans*-disubstitution of two carboxylate by *N*,*N*′-di-*p*-anisylformamidinate (DAniF) ligands is easily achieved due to their strong *trans*-directing influence. The stronger binding of the amidinate ligands also allows for subsequent exchange of the remaining carboxylate ligands with preservation of the *trans*-configuration. In contrast, direct carboxylate substitution in paddle-wheel complexes $M_2(O_2CR)_4$ by other carboxylates is generally unselective.

More recently, *trans*-disubstitution has allowed for the preparation of paddle-wheel complexes that offer a defined pathway for charge transport along the molecular backbone. Since the paddle-wheel motif is one of the few structural templates where the metal-metal bond order can be systematically tuned, it offers the rare opportunity to investigate, whether a direct connection to charge conductance exists. First forays into this topic were reported by the groups of Liu

[a] A. Mang, M. Linseis, R. F. Winter
Fachbereich Chemie, Universität Konstanz, 78457 Konstanz, Germany
E-mail: rainer.winter@uni-konstanz.de

Supporting information for this article is available on the WWW under https://doi.org/10.1002/zaac.202200199

Journal of Inorganic and General Chemistry
ZAAC
Zeitschrift für anorganische und allgemeine Chemie

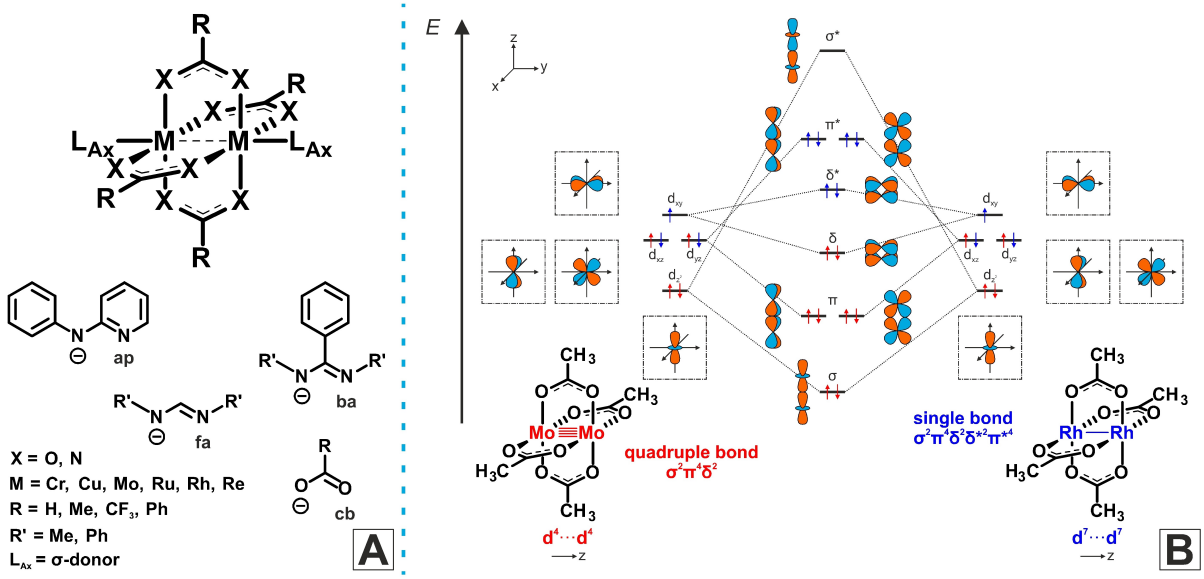

Scheme 1. (**A**) General structure of a paddle-wheel complex comprising a central dinuclear metal core, four laterally attached bridging chelate ligands RCX_2^- (ap = anilinopyridinate, ba = benzamidinate, fa = formamidinate, cb = carboxylate) and two axial ligands (L_{Ax}). (**B**) Molecular orbital scheme indicating the pairwise interactions of the metal d-orbitals of the dimetal core. The different electronic occupations for molybdenum(II) and rhodium(II) acetate are shown in red and blue colours, respectively.

and Hong, who prepared and investigated the anchor group-modified paddle-wheel complexes *trans*-$Mo_2(DAniF)_2(^i nic)_2$ and *trans*-$Mo_2(DAniF)_2(nic)_2$ (^{i}nic = isonicotinate; nic = nicotinate).[10] Molecular conductance studies employing the scanning tunneling microscope break-junction (STM-BJ) technique revealed, that the conductances of the paddle-wheel complexes surpass those of their organic congeners 1,4-bis(4-pyridyl)benzene and 1,4-bis(3-pyridyl)benzene by more than one order of magnitude despite the significantly increased molecular length. Their superior performance was attributed to efficient d(δ)-p(π) conjugation between the dimolybdenum core and the *trans*-disposed π-conjugated ligand backbone.

The molecular conductance properties of the heteroleptic molybdenum paddle-wheel complexes encouraged us to embark on a study aimed at exploring the single-molecular charge transport properties of related rhodium(II) based complexes with their $\sigma^2\pi^4\delta^2\delta^{*2}\pi^{*4}$ electron configuration and the Rh–Rh bond order of one (see panel B, Scheme 1). At difference to the work of Liu and Hong, we sought to align the conduction pathway with the metal-metal bond vector and hence to establish molecule-electrode contacting through the axial coordination sites L_{Ax} of a $Rh_2(OAc)_4(L_{Ax})_2$ bis(adduct) (see panel A, Scheme 1). This can in principle be done by attaching a ditopic, anchor group-modified σ-donor ligand to each metal terminus of the paddle-wheel complex. Our approach thus follows reports by Liu *et al.*, who investigated the charge transport properties of coordination polymers of rhodium paddle-wheel complexes. The latter were formed through a layer-by-layer assembly, by interconnecting rhodium paddle-wheels with pyrazine or (*E*)-1,2-di(pyridin-4-yl)ethene bridging ligands, starting from a first layer that was immobilised on a gold substrate by 2-(4-pyridyl)ethanethiol anchors.[11] Similarly to them, we initially employed 4-methylthio-functionalised pyridine (PySMe) and prepared the respective rhodium(II) acetate κN–$NC_5H_4SCH_3$ bis(adduct) $Rh_2(OAc)_4(PySMe)_2$ (Scheme 2, panel B). This binding mode should leave the methylthio groups available for contacting the molecule through the formation of S–Au linkages at the electrode-molecule interfaces in STM-BJ experiments.

Although $Rh_2(OAc)_4(PySMe)_2$ appeared to be stable in solution, STM-BJ studies were thwarted by easy cleavage of the pyridine N–Rh bonds in favour of apparently more stable N–Au interactions. Hence, the conductance signatures exclusively corresponded to those of the detached PySMe ligand. Such behaviour was independently observed by Doerrer, Kamenetska and their coworkers for homo- and heterobimetallic paddle-wheel complexes of the type $PtM(tba)_4(PySMe)$ (tba = thiobenzoate; M = Mn, Fe, Co, Ni, Zn), $PtM(SAc)_4(PySMe)$ (SAc = thioacetate; M = Co, Ni, Zn) and $Cu_2(OAc)_4(PySMe)_2$ with the same anchor group-modified pyridine ligand.[12] Thus, axial functionalisation of paddle-wheel complexes for single-molecule conductance measurements has so far remained elusive.

We felt that this might be remedied by introducing axial ligands that are capable of forming strong N–H···O hydrogen bonds to the equatorial carboxylate donors. Apart from strengthening the bonding of axially coordinated ligands to the paddle-wheel core, secondary N–H···O interactions might also serve to further enhance their conductance properties, as charge transport over hydrogen bonds is known to exceed that over σ-channels at short ranges.[13]

In this contribution we present four different anchor group-functionalised ligands **L1**–**L4** and their respective rhodium(II) acetate bis(adducts) **C1**–**C4** for subsequent application in STM-BJ single-molecule charge transport studies.

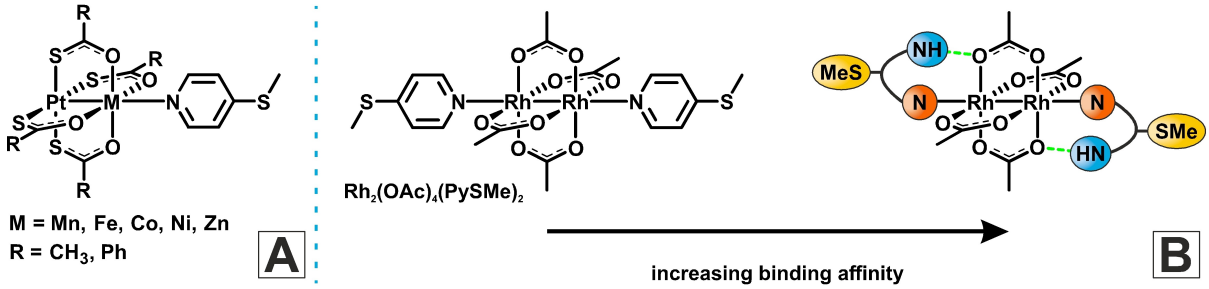

Scheme 2. (**A**) Heterobimetallic paddle-wheel complexes investigated by Doerrer, Kamenetska and coworkers.[12] (**B**) Structure of the bis(adduct) $Rh_2(OAc)_4(\kappa N\text{–PySMe})_2$ (left) and schematic drawing of a hydrogen bond-supported paddle-wheel bis(adduct) with enhanced Rh–L_{Ax} binding to prevent ligand dissociation in STM-BJ experiments (right).

Their synthesis, spectroscopic features (NMR, IR, vis), crystal structures and a DFT-based assay of their crucial frontier molecular orbitals and the impact of hydrogen bonding on the strength of the Rh-L_{Ax} bond as well as a comparison of the energies of *cis*- and *trans*- or the κN- and κS-linkage isomers will be discussed in the following.

Results and discussion

Initial considerations and ligand design

The choice of appropriate ligands was based on the following considerations: i) Any type of ligand with a RN=CR′–NHR functionality should qualify as it features both, a σ-donor and a hydrogen bond donor entity. ii) The ligand backbone must allow for anchor group functionalisation in order to establish a reliable molecule-electrode contact for conductance measurements. iii) In order to achieve high conductance values, the ligands should offer an uninterrupted π-(cross-)conjugated conduction pathway along the entire molecular backbone. All these requirements are met with ligands **L1**–**L4** (Scheme 3).

Our choice of the methylthio function roots in its known ability to establish robust links to surface atoms of the gold STM tip and substrate.[14] In addition, thioethers are insensitive towards basic and acidic conditions and consequently provide chemical stability during ligand synthesis. We already note that ligands **L3** and **L4** may also bind as κS-donors while still being capable of establishing additional N–H···O hydrogen bonds. They hence generate ambiguity with respect to which of the different donor atoms preferably binds to rhodium.

Synthesis

Ligands **L1**–**L4** were synthesised starting from commercially available starting materials by the two- to four-step procedures outlined in Scheme 4. Detailed synthetic protocols are provided in the Experimental Section. *N*,*N*′-Dimethyl-4-(methylthio)benzamidine (**L1**) was prepared in an overall yield of 19% over four steps *via* a double chlorination-substitution sequence starting from 4-methylthiobenzoic acid (**1**), following established literature procedures.[15] The obtained benzamidine **L1** was purified by a modified work-up protocol involving protonation of the free ligand to the corresponding benzamidinium salt **L1**·**HCl**, aqueous extraction and precipitation by treatment with NaOH base. **L1** readily formed colourless crystals from acetone solution.

Anilinopyrimidine-derived ligand **L2** was accessible in two steps starting from 2,4-dichloropyrimidine (**5**).[16] Cooling and maintaining a low concentration of the methyl thiolate solution proved essential for selective monosubstitution of the 4-chloro-substituent during the first synthesis step. For isothiourea derivatives **L3** and **L4**,[17] the methylthio group was introduced through methylation of the thiourea functionality of precursors **7** and **9**, followed by deprotonation with concentrated aqueous ammonia.

The target paddle-wheel complexes **C1**–**C4** were accessible by treating dirhodium(II) tetraacetate (**11**) with the respective donor ligands **L1**–**L4** in a 1:2 molar ratio in dichloromethane solution at room temperature (Scheme 5).[18] For this purpose, pristine **11** was freshly prepared by heating the bis(methanol) adduct $Rh_2(OAc)_4\times 2$ MeOH under reduced pressure, which removes the axial solvento ligands. This is accompanied by a

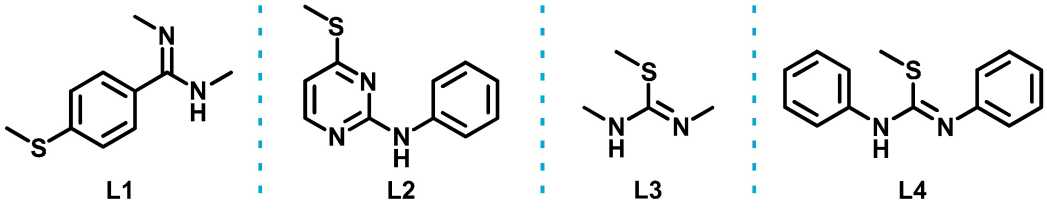

Scheme 3. Methylthio-functionalised donor ligands **L1**–**L4** that are capable of forming Rh-imine and N–H···O hydrogen bonds.

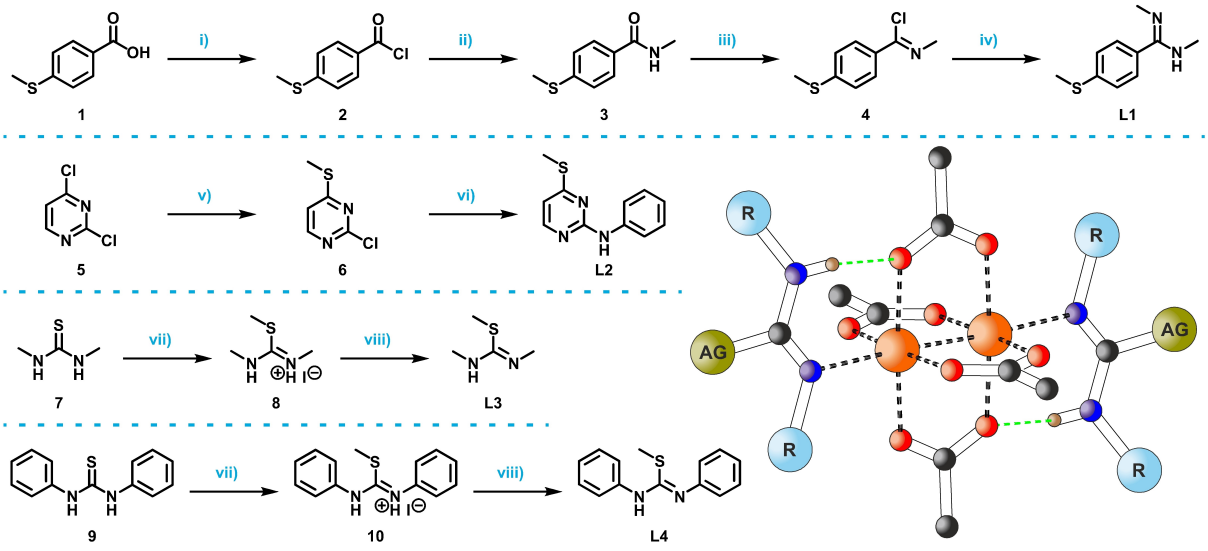

Scheme 4. Synthetic pathway towards the hydrogen bond-donor ligands **L1**–**L4** (left) and schematic depiction of their hydrogen bond-supported coordination to dirhodium tetraacetate (right). Reaction conditions: i) $SOCl_2$, reflux, 3 h, quant.; ii) $MeNH_3Cl$, K_2CO_3, ethyl acetate/H_2O (2:1 *v/v*), 0 °C to r.t., 7 h, 92 %; iii) $SOCl_2$, reflux, 4 h, 76 %, iv) $MeNH_3Cl$, NaOH, H_2O, 0 °C to r.t., 17 h, 27 %; v) NaSMe, DMF, 0 °C to r.t., 17 h, 34 %; vi) aniline, neat, 120 °C, 2 h, 82 %; vii) MeI, acetone, r.t., 16 h, **8**: 76 %, **10**: 84 %; viii) conc. $NH_{3(aq)}$, H_2O, 0 °C to r.t., 1 h, **L3**: 50 %. **L4**: 97 %.

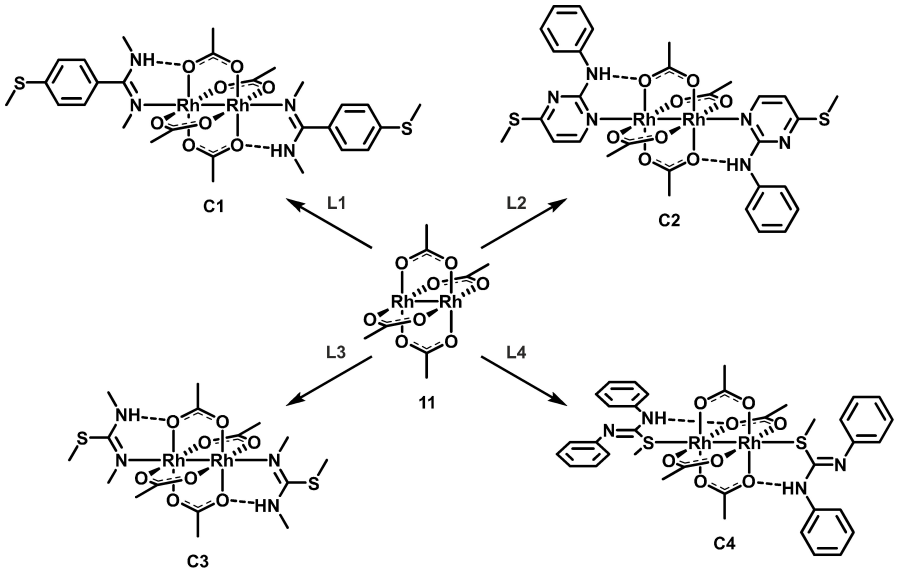

Scheme 5. Synthetic pathway towards the hydrogen bond-supported dirhodium paddle-wheel bis(adducts) **C1**–**C4**. General reaction conditions: $Rh_2(OAc)_4$ (1.00 eq.), **L1**–**L4** (2.00 eq.), CH_2Cl_2, r.t., 1 h. The purification routine involved crystallisation of the bis(adducts) by layer diffusion of *n*-pentane into a saturated solution of the respective complex in CH_2Cl_2.

distinct change in colour from dark blue to emerald green. Bis(adduct) formation with **L1**–**L4** was likewise indicated by an immediate colour change from emerald green to magenta (**C1**, **C3**), red (**C2**), or purple (**C4**). All complexes were obtained in moderate to good yields (**C1**, 78 %; **C2**, 49 %; **C3**, 46 %; **C4**, 80 %) as crystalline solids *via* layer diffusion of *n*-pentane into saturated solutions of **C1**–**C4** in dichloromethane. The obtained single crystals proved suitable for X-ray analysis.

Spectroscopic studies

Ligands **L1**–**L4** and the paddle-wheel bis(adducts) **C1**–**C4** were characterised by ^{1}H-NMR spectroscopy in CD_2Cl_2 or $CDCl_3$ solution at room temperature. ^{1}H-NMR spectra of the **L2**–**C2** and **L4**–**C4** pairs of compounds are shown in Figure 1 and relevant ^{1}H resonances are listed in Table 1. A complete collection of NMR spectra can be found in the Supporting Information. The methylthio functionality, which is common to

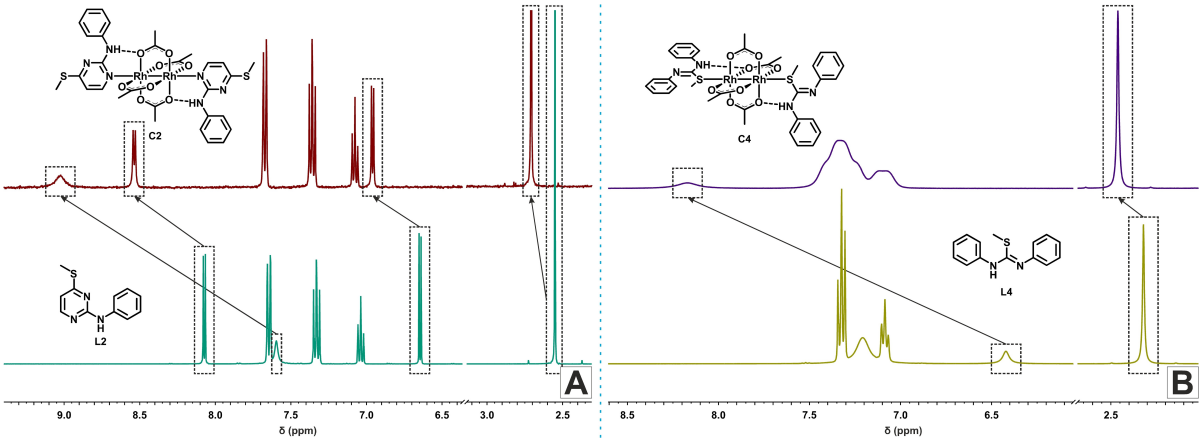

Figure 1. ^{1}H-NMR (400 MHz, CD_2Cl_2, r.t.) spectra of the ligand-complex pairs **C2**–**L2** (**A**) and **C4**–**L4** (**B**) indicating the downfield shifts of characteristic ligand resonances upon bis(adduct) formation.

Table 1. The most important ^{1}H-NMR (400 MHz, CD_2Cl_2, r.t.) resonances of ligands **L1**–**L4** and of complexes **C1**–**C4**, as well as coordination shifts $\Delta\delta_{Cx-Lx}$ upon bis(adduct) formation.

^{1}H-Resonance	L1	C1	$\Delta\delta_{C1-L1}$	L2	C2	$\Delta\delta_{C2-L2}$	L3	C3	$\Delta\delta_{C3-L3}$	L4	C4	$\Delta\delta_{C4-L4}$
δ_{SMe} (ppm)	2.49	2.62	0.13	2.55	2.71	0.16	2.33	2.58	0.25	2.32	2.46	0.14
δ_{N-H} (ppm)	4.11	6.49	2.38	7.60	9.02	1.42	4.19	5.82	1.63	6.42	8.17	1.75

all ligands, gives rise to a characteristic singlet resonance at $\delta = 2.50$ ppm for aromatic ligands **L1** and **L2** or at ca. 2.3 ppm for isothioureas **L3** and **L4** (see Table 1). Owing to the different chemical nature of the amine functions in ligands **L1**–**L4**, shift variations for the N–*H* proton are appreciably larger and range from 4.11 ppm or 4.19 ppm in **L1** and **L3** to 6.42 ppm in the *N*,*N*′-diphenyl-substituted isothiourea **L4**, and to even 7.60 ppm in anilinopyrimidine **L2**.

All these resonances experience distinct low-field shifts upon coordination to the $Rh_2(OAc)_4$ core (see Figure 1 and Table 1). As is expected for the formation of N–H···O hydrogen bonds, this is particularly evident for the N–*H* proton, where the shift difference $\Delta\delta$ amounts to 1.42 ppm to 2.38 ppm. The N–*H* shift differences for individual complex-ligand pairs decrease in the order **C1**–**L1** > **C4**–**L4** > **C3**–**L3** > **C2**–**L2**, which suggests that the strength of the N–H···O hydrogen bond to an acetate ligand increases from anilinopyrimidine to isothiourea and benzamidine. A conspicuous feature in the NMR spectra (see panel B in Figure 1 and the Supporting Information) is a general broadening of resonances, in particular those of the N–*H* proton and of the resonances of the N–*Ph* moieties, particularly in **C4**. This is suggestive of dynamic behaviour on the NMR timescale, which may include "on-off" equilibria with a cleavage of N–H···O hydrogen bond(s) or equilibration between *cis*- and *trans*-isomers with regard of the positioning of the acetate ligands that serve as the hydrogen bond acceptors (*vide infra*). No safe conclusions as to whether the isothiourea ligands in complexes **C3** and **C4** coordinate in a κS- or a κN-fashion can be drawn from the NMR spectra.

In addition to the low-field shifts in ^{1}H-NMR spectroscopy, the formation of intramolecular N–H···O hydrogen bonds also leads to distinct changes in the energy and shape of the N–H vibrations in the IR spectra. Typically, hydrogen bonding causes X–H band shifts to lower wavenumbers and a notable increase in IR intensities. The magnitude of this shift commonly scales with the strength of the hydrogen bond.[19] IR spectra recorded from KBr pellets are illustrated in the Supporting Information. Excerpts for each ligand-complex pair are provided in Figure 2 while the relevant IR data are collected in Table 2.

As is evident from panels A–D in Figure 2, the free ligands **L1**–**L4** show a characteristic N–H band in the range of 3190 cm^{-1} to 3390 cm^{-1}. The breadth of this band and a consistent, large red shift from the DFT-calculated frequencies of the ν(N–H) stretch for an isolated molecule in CH_2Cl_2 (see Table 2)[20] suggest, that the respective bands correspond to the ν(N–H···N′) modes of hydrogen-bonded dimers or chainlike aggregates[21] as they are, for example, present in crystalline *N*,*N*′-di-*p*-tolylbenzamidine,[22] *N*,*N*′-diphenyl-4-(methoxy)benzamidine[23] or imino-substituted benzamidines.[24] The potential presence of *Z*- and *E*-isomers with respect to the C=N bond in the isothioureas **L3**, **L4** and benzamidine **L1** may also contribute to the rather large width and asymmetrical shape of the N–H band.[21]

Upon metal coordination, the indicated bands are replaced by a much sharper band at 3320 cm^{-1} (**C1**), 3348 cm^{-1}(**C2**), 3334 cm^{-1} (**C3**) or 3279 cm^{-1} (**C4**), respectively. Except for the **L3**/**C3** pair of compounds, we note a blue shift of the N–H band on metal coordination. In agreement with the results

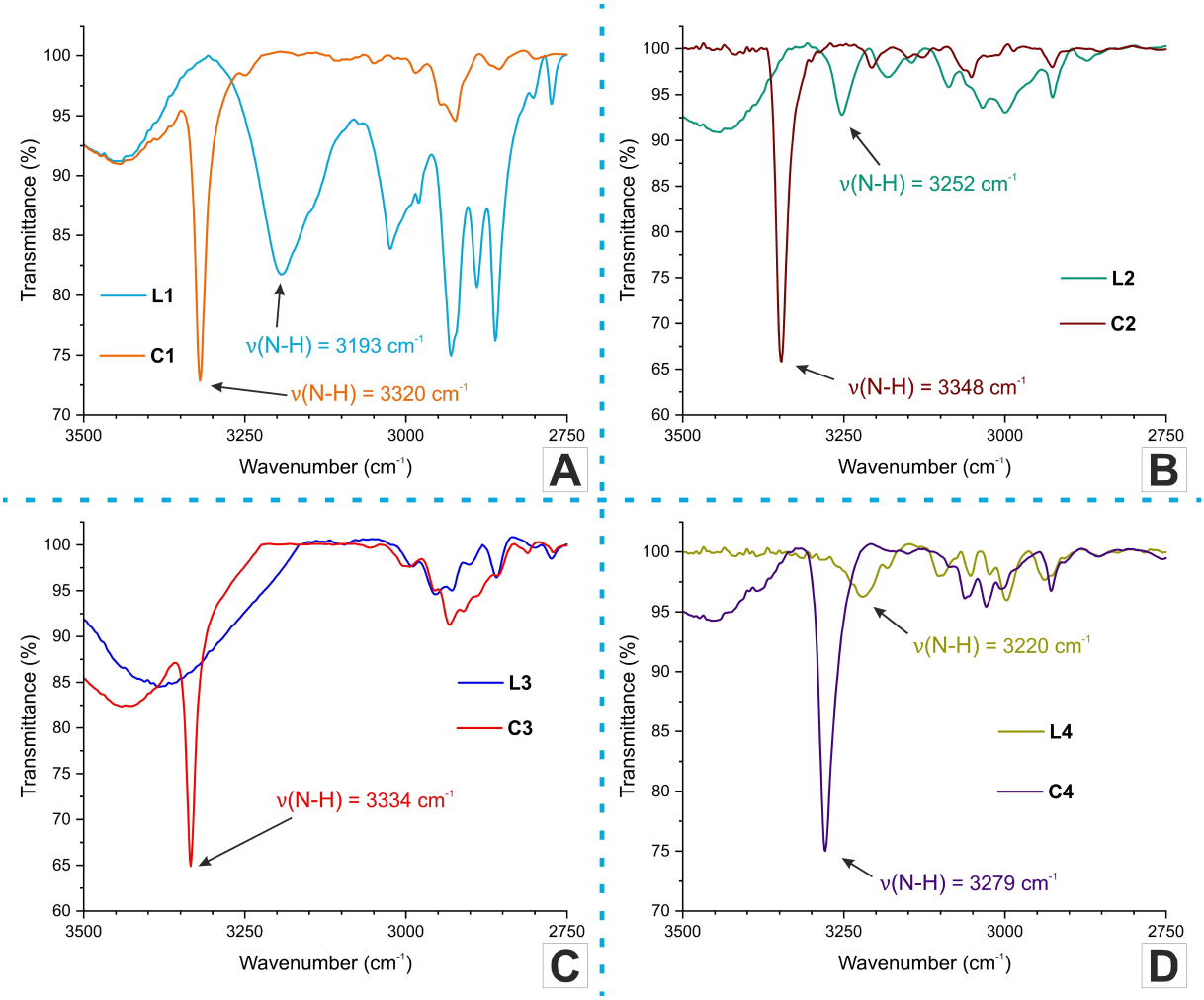

Figure 2. Relevant excerpts of the IR spectra (KBr pellets) of the corresponding ligand-complex pairs **L1**–**C1** (**A**), **L2**–**C2** (**B**), **L3**–**C3** (**C**) and **L4**–**C4** (**D**), respectively.

Table 2. DFT-computed and experimental IR data for hydrogen bond donor ligands **L1**–**L4**, rhodium(II) acetate (**11**) and the derived bis(adducts) $Rh_2(OAc)_4(L_{Ax})_2$, **C1**–**C4**. Differences Δν are provided as absolute values.

	Vibrational modes (cm^{-1})								
	ν(C=O) (cm^{-1})			ν(C=N) (cm^{-1})			ν(N–H) (cm^{-1})		
Compound	Exp.	Calc.[a]	Δν	Exp.	Calc.[a]	Δν	Exp.	Calc.[a]	Δν
11	1577	1586	9	–	–	–	–	–	–
L1	–	–	–	1621	1659	38	3193	3475	282
C1	1589	1597	8	1633	1628	5	3320	3374	54
L2	–	–	–	1557	1548	9	3252	3457	205
C2	1582	1593	11	1549	1552	3	3348	3366	18
L3	–	–	–	1612/1624[c]	1653	41/29	n. i.[b]/3462[c]	3398	–/64
C3	1589	1596	7	1607	1618	11	3334	3345	11
L4	–	–	–	1575	1642	67	3220	3498	278
C4	1587	1591	4	1559	1658	99	3279	3352	73

(a) Computed vibrational energies were corrected for their offset in zero-point energies with the recommended scaling factor of 0.9512 for the employed PBE1PBE/6-31G(d) combination of functional and basis set functions.[25] (b) Not identifiable due to overlap with the band of residual water in KBr. (c) Measured in dichloromethane solution.

from X-ray crystallography (*vide infra*), these bands are ascribed to ν(N–H···O) of an amine N–H functionality, which is hydrogen-bonded to a carboxylate. The significant narrowing and intensity increase of ν(N–H) are indicative of strong

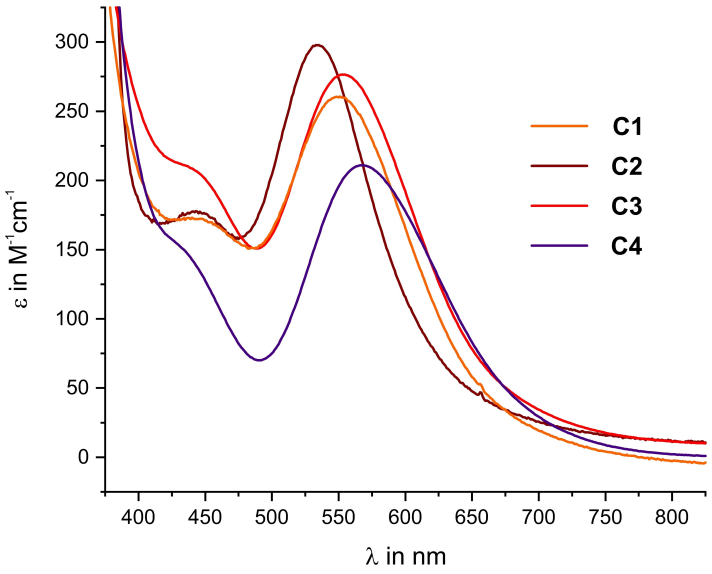

Figure 3. Electronic absorption spectra of complexes **C1**–**C4** measured in dichloromethane solution at r.t.

intramolecular hydrogen bonding in the paddle-wheel bis(adducts).

The different colour impressions induced by variation of the axial ligands L_{Ax} also prompted us to study their electronic spectra in energy range of visible light (vis). The results are provided in Figure 3 and Table 3. After considerable debate,[26] the so-called A band at the lowest energy, which is highly sensitive to the identity of the axial ligands,[18c,27] was ultimately assigned as the d(π^*, Rh_2)→d(σ^*, Rh_2) excitation.[27–28] As such, better σ-donors and/or π-acceptors will increase the HOMO-LUMO gap and hence shift this band to higher energy. The second band, usually referred to as the B band, is largely invariant to axial ligand modifications and is due to a transition from the same Rh–Rh dπ* orbitals to orbitals that are σ-antibonding with respect to the Rh–O bonds of the equatorial carboxylate donors (d(π^*, Rh_2)→d(σ^*, Rh–O)).

Consistent with earlier considerations, complex **C2** with the strongest π-accepting pyrimidine ligand has the most blue-shifted A band, followed by complex **C1** with weaker π-acidic benzamidine ligand. Complex **C3** absorbs at almost identical energy. This supports the notion that the thiourea ligand **L3** also coordinates *via* its imine *N* donor. The deviating energy of the A band in complex **C4** is thus suggestive of the alternative κ*S* binding mode.

Table 3. Characteristic absorption data of complexes **C1**–**C4** in the visible range.

Complex	λ_{max} in nm (ε_{max} in $M^{-1}cm^{-1}$)
C1	551 (261), 440 (173)
C2	535 (298), 443 (178)
C3	553 (277), 432 (212)
C4	568 (211), 428 (155)

Crystallographic studies

Ligand **L1** formed well-shaped colourless blocks, which allowed for the investigation of its molecular structure and analysis of intermolecular interactions in the crystal. The investigated specimen crystallised in the orthorhombic space group *Pbca* with eight formula units per unit cell. The molecular structure is shown in panel A of Figure 4 while Table 4 provides the corresponding crystallographic information along with pertinent bond lengths, bond angles and torsion angles. In the crystal lattice, **L1** is present as the *E,Z*-isomer with the methyl substituent at the imine nitrogen atom N1 pointing to the side of the 4-(methylthio)phenyl substituent at the central carbon atom (*E*) and the methyl substituent at the amine N atom N2 oriented to the same side as the imine nitrogen atom (*Z*).

The central carbon atom C2 is sp^2-hybridised as is indicated by the planar N1=C2–N2–C4 entity in concert with the bond angles N1=C2–N2 of 119.38(14)°, N1=C2–C4 of 126.76(14)° and N2–C2–C4 of 113.82(13)° and an angle sum of 359.96°. The rather long imine-carbon bond N1=C2 of 1.292(2) Å and the short amine N2–C2 bond of 1.352(2) Å comply with the notion of n-π conjugation along the RN–C(R′)=NR″ backbone as it is typical for amidines.[23,29] The phenyl ring is rotated out of the N=C–N plane by 51.9(2)° (N1=C2–C4–C5).

Benzamidines constitute self-complimentary building blocks as they feature a hydrogen bond donor (N–H) as well as an imine hydrogen bond acceptor R–N=CR′ within the same molecule. In the case of **L1**, N–H···N′ hydrogen bonding associates individual molecules into infinite 1D chains that run along the *a*-axis of the unit cell with N2···N1′ = 2.871 Å, a short intermolecular N2–H···N1′ hydrogen bond distance of 2.106 Å and a N2–H···N1′ angle of 147.9° (see the panels B and C of Figure 4). Such chain motifs are also present in other *N,N′*-dimethyl-substituted benzamidines such as the simple phenyl

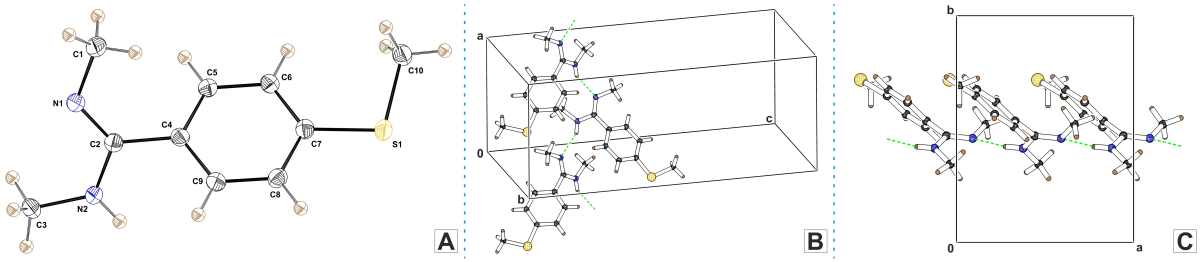

Figure 4. (**A**) ORTEP of *N*,*N*′-dimethyl-4-(methylthio)benzamidine (**L1**). Thermal ellipsoids are displayed at a 50% probability level. (**B**) Part of the packing structure of **L1** involving the defined intermolecular hydrogen bond network along the *a*-axis of the unit cell. Only one fourth of the cell contents are shown for clarity reasons. (**C**) View on the *ab*-plane along the *c*-axis.

Table 4. Crystallographic data (left) and selected bond parameters (right) of *N*,*N*′-dimethyl-4-(methylthio)benzamidine (**L1**) in the solid state. Bond lengths are given in Å, interatomic angles in deg. (°) and torsion angles as absolute values in deg. (°).

	L1	Distance/angle / torsion angle	Value (Å/°)
Empirical formula	$C_{10}H_{14}N_2S$	C1–N1	1.459(2)
Formula weight (g/mol)	194.29	N1–C2	1.292(2)
Temperature (K)	100	C2–N2	1.352(2)
Crystal system	orthorhombic	N2–C3	1.442(2)
Space group	*Pbca*	C2–C4	1.494(2)
a (Å)	8.5975(3)	C7–S1	1.7645(17)
b (Å)	10.9568(4)	N1–S1	6.9564(14)
c (Å)	21.4309(11)	N2–S2	6.6643(14)
α (°)	90	N1–C2–N2	119.38(14)
β (°)	90	C7–S1–C10	103.48(8)
γ (°)	90	N1–C2–C4–C5	51.9(2)
Volume (Å^3)	2018.81(15)	C6–C7–S1–C10	14.90(6)
Z	8	N–H···N′	2.106
Independent reflections	2487		
R_{int}	0.0181		
R_{sigma}	0.0180		
Goodness-of-fit on F^2	1.107		
Final *R* indexes [$I \geq 2\sigma$ (I)]	$R_1 = 0.0361$, $wR_2 = 0.0831$		
Final *R* indexes [all data]	$R_1 = 0.0492$, $wR_2 = 0.0987$		

derivative and its 3-trifluoromethyl-, 3-methoxy-, 4-bromo-, 4-iodo- and 4-nitro-substituted congeners.[15c,30] Within every chain, the phenyl rings alternately point to different sides (Figure 4, panel B). Chains of molecules associated by N2–H···N hydrogen bonding stack along the *b*-axis of the unit cell and associate *via* C–H···π interactions of 2.756 Å between phenyl proton H8 and the amidine carbon atom C2. Stacks of so-associated chains repeat along the *c*-axis of the unit cell in an alternant, antiparallel, offset fashion. Between these neighbouring chains, pairwise C–H···π interactions of 2.719 Å between proton H10B of the methylthio group and carbon atom C6 of the phenyl substituent are established. Graphic representations of the hydrogen bonding motifs present in crystalline **L1** are shown in Figure S24 of the Supporting Information.

Complex **C1** crystallises in the triclinic space group $P\bar{1}$ with a single formula unit per unit cell. An ORTEP of **C1** is presented in panel A of Figure 5, while crystallographic details, together with those of the other complexes, are provided in Table 5. Table 6 lists the most important bond lengths, bond angles and torsion angles. Further relevant data are available in the Supporting Information. Two ligands **L1** occupy the axial coordination sites at the metal termini. As desired, **L1** coordinates with its imine donor with the N–H proton oriented towards one of the carboxylate ligands, thereby establishing a N–H···O hydrogen bond. An inversion center located at the midpoint of the Rh–Rh bond positions the amidines in an antiparallel fashion.

The Rh1–Rh1′ distance in **C1** measures 2.4200(3) Å, which is somewhat longer than that of 2.3860(30) Å in the related aquo complex $Rh_2(OAc)_4(H_2O)_2$,[2] but similar to those observed in the related *N*,*N*′-di-*p*-tolylformamidine (d_{Rh-Rh} = 2.4120(8) Å)[31] or 1,3-diphenyltriazene derivatives (d_{Rh-Rh} = 2.407(2) Å).[32] Metal coordination leaves the C=N and the C–N bond lengths of **L1** unaltered; the values of 1.288(3) Å for N1=C5 and of 1.357(3) Å for N2-C5 are virtually identical to those of free **L1**. As opposed to the free ligand, the N–H proton of the amidine ligands exclusively forms an intramolecular N–H···O hydrogen bond with a contact N2···O2 of 2.779(3) Å and d(N2–H···O2) = 1.97 Å. The latter is significantly

Journal of Inorganic and General Chemistry
ZAAC
Zeitschrift für anorganische und allgemeine Chemie

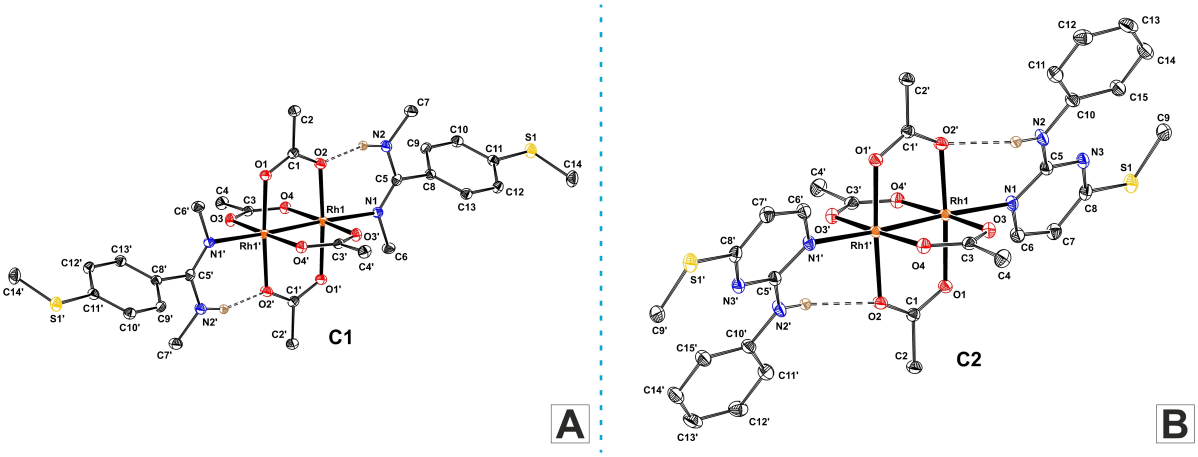

Figure 5. ORTEP of (**A**) the rhodium(II) acetate bis(*N*,*N*′-dimethyl-4-(methylthio)benzamidine) adduct **C1** and (**B**) rhodium(II) acetate bis(4-(methylthio)-*N*-phenylpyrimidine-2-amine) adduct **C2**. Thermal ellipsoids are displayed at a 50 % probability level. Hydrogen atoms (except for N–H) and co-crystallised solvent molecules are omitted for clarity reasons.

Table 5. Crystallographic data for complexes **C1**–**C4**.

Parameter	**C1**	**C2**×CH_2Cl_2	**C3**	**C4**
Empirical formula	$C_{28}H_{40}N_4O_8Rh_2S_2$	$C_{31}H_{36}Cl_2N_6O_8Rh_2S_2$	$C_{16}H_{32}N_4O_8Rh_2S_2$	$C_{36}H_{40}N_4O_8Rh_2S_2$
Formula weight (g/mol)	830.58	961.50	678.39	926.66
Temperature (K)	100	100	100	100
Crystal system	triclinic	monoclinic	triclinic	monoclinic
Space group	$P\bar{1}$	$C2/c$	$P\bar{1}$	$C2/c$
a (Å)	7.5291(5)	23.8867(8)	7.2513(6)	26.4429(7)
b (Å)	8.7156(5)	10.1235(2)	8.0943(6)	10.2329(4)
c (Å)	13.3196(8)	14.9327(5)	11.1869(10)	14.0021(4)
α (°)	99.369(5)	90	99.970(7)	90
β (°)	98.369(5)	91.707(3)	104.962(7)	98.739(2)
γ (°)	109.640(5)	90	95.545(6)	90
Volume (Å^3)	792.46(9)	3609.38(19)	617.84(9)	3744.8(2)
Z	1	4	1	4
Independent reflections	3613	4135	5824	4303
R_{int}	0.0980	0.0201	0.0403	0.0214
R_{sigma}	0.0708	0.0143	0.0221	0.0195
Goodness-of-fit on F^2	1.045	1.064	1.186	1.050
Final R indexes [$I \geq 2\sigma$ (I)]	$R_1 = 0.0296$, $wR_2 = 0.0619$	$R_1 = 0.0210$, $wR_2 = 0.0486$	$R_1 = 0.0506$, $wR_2 = 0.1347$	$R_1 = 0.0273$, $wR_2 = 0.0701$
Final R indexes [all data]	$R_1 = 0.0354$, $wR_2 = 0.0659$	$R_1 = 0.0235$, $wR_2 = 0.0504$	$R_1 = 0.0605$, $wR_2 = 0.1810$	$R_1 = 0.0312$, $wR_2 = 0.0745$

shorter than the intermolecular N–H···N′ contacts of 2.106 Å in **L1**. Similar observations were made in various other $Rh_2(OAc)_4(L_{Ax})_2$ paddle-wheel complexes with imine donors featuring additional N–H functionalities that are capable of forming intramolecular hydrogen bonds to acetate ligands. Examples are the di-*p*-tolylformamidine[31] or 1,3-diphenyltriazene complexes[32] and bis(adducts) with axial 7-azaindole ligands. In these examples, intramolecular N···O contacts range from 2.720 Å to 2.886 Å.[33] The shortened hydrogen bond and its increased linearity (156.0° *vs.* 147.9°) are tokens of an increased bond strength as compared to the N–H···N′ interactions in uncoordinated **L1**.

Hydrogen bonding also leaves its marks on the Rh–O bond lengths. Their engagement in hydrogen bonding deprives the oxygen donor atoms O2 of some electron density, so that Rh1–O2 of 2.0526(16) Å represents the longest of all Rh–O bonds. This is counterbalanced by a shortening of the Rh1′–O1 bond to the other oxygen atom of the same carboxylate ligand to 2.0389(16) Å. Rh–O bond lengths to the other acetates that do not engage in N–H···O hydrogen bonding fall in between these two values and measure 2.0449(19) Å (Rh1–O3′) and 2.0446(17) Å (Rh1–O4). The N2–H···O2 interactions between the N–H functionality of the amidine moieties and the laterally coordinated, bridging acetate ligands establish irregular six-membered

Table 6. Selected bond parameters for the four paddle-wheel complexes **C1**–**C4** in the solid state. Bond lengths are given in Å, interatomic angles in deg. (°) and torsion angles as absolute values in deg. (°).

Distance/angle/torsion angle	**C1**[(a)]	**C2**×CH_2Cl_2[(a)]	**C3**[(a)]	**C4**[(b)]
Rh1–Rh1′	2.4200(3)	2.4013(5)	2.4043(11)	2.3983(6)
Rh1–O1′/Rh1–O1	2.0389(16)	2.0299(12)	2.051(6)	2.0356(15)
Rh1–O2/Rh1–O2′	2.0526(16)	2.0472(12)	2.052(7)	2.0299(15)
Rh1–O3′/Rh1–O3	2.0449(19)	2.0339(13)	2.040(7)	2.0354(15)
Rh1–O4/Rh1–O4′	2.0446(17)	2.0475(13)	2.033(6)	2.0499(15)
Rh1–N1/Rh1–S1	2.299(2)	2.2741(15)	2.248(8)	2.5158(7)
N1–C5	1.288(3)	1.357(2)	1.273(12)	1.272(3)
N1–C6	1.467(3)	1.341(2)	1.461(12)	–[(c)]
C5–N2	1.357(3)	1.357(2)	1.390(13)	1.363(3)
N2–C7	1.453(3)	–[(c)]	1.453(14)	–[(c)]
N···O	2.7840(14)	2.8830(19)		
N1···N1′	7.016(3)	6.947(2)	6.900(11)	11.386(3)
S1···S1′	20.7819(17)	15.8487(8)	12.069(3)	7.4091(8)
N1–Rh1–O2/N1–Rh1–O2′/S1–Rh1–O2′	96.42(7)	95.58(5)	93.9(3)	84.97(5)
O1′–Rh1–O2/O1–Rh1–O2′	174.95(7)	175.69(5)	175.7(3)	175.57(7)
O2–Rh1–O4/O2′–Rh1–O4′	91.38(6)	90.42(5)	89.0(3)	86.44(6)
Rh1–N1–C5/Rh–S1–C5	126.89(19)	128.16(11)	125.5(7)	111.91(7)
Rh1–N1–C5–N2/Rh1–S1–C5–N2	2.9(4)	4.5(2)	9.1(12)	35.20(17)
O2–Rh1–N1–C5/O2′–Rh1–N1–C5/O3–Rh1–S1–C5	2.1(2)	23.65(14)	43.2(8)	58.17(9)
O4–Rh1–N1–C5/O4′–Rh1–N1–C5/O1–Rh1–S1–C5	89.5(2)	114.40(14)	132.2(8)	122.08(9)
O1′–Rh1–N1–C5/O1–Rh1–N1–C5/O4′–Rh1–S1–C5	178.2(2)	156.53(14)	136.2(8)	28.18(9)
N–H···O	1.97	2.08	2.40	2.20

(a) The asymmetric unit of **C1**, **C2** and **C3** exhibits an inversion center located at the midpoint of the Rh–Rh bond. Therefore, all data for parameters X–Y′ correspond to the inverted pairing X′–Y. (b) For **C4**, the symmetry-equivalent carboxylate ligands are *cis*-disposed. (c) No connectivity among the specified atoms.

Rh1–O2···H–N2–C5=N1 rings with the complimentary Rh1–O2 part of the paddle-wheel structure. The plane spanned by the N1=C5–N2 entity is nearly coplanar to the five-membered metallacyclic Rh1–Rh1′–O1–C1–O2 ring as indicated by an interplanar angle of only 3.52° and a small O2–Rh1–N1=C5 torsion of 2.1(2)°. Such features are also present in other $Rh_2(OAc)_4(L_{Ax})_2$ paddle-wheels with intramolecular hydrogen bonding. However, no general correlation between the interplanar angle as defined above and the N···O distance between the N–H hydrogen bond donor and the acetate hydrogen bond acceptor seems to exist, as is indicated by a considerable spread (e.g. d(N···O) = 2.7840(14) Å with an interplanar angle of 27.60° in the diphenyltriazene complex[32] or d(N···O) = 2.873 Å with an interplanar angle of 20.25° in the bis((2-pyridyl)amine) complex[34] versus d(N···O) = 3.003 Å with an interplanar angle of 8.81° in a mercaptopurine bis(adduct)).[35] Such coplanar orientation should, in principle, be advantageous for charge transmission. This might, however, be counterbalanced by a large tilt of the phenyl ring at the amidine C5 atom of 65.8(4)°. Another important parameter for the application in charge transport studies is the overall distance between the thioether anchor groups (d(S1···S1′)) in **C1**, which amounts to 20.7819(17) Å. **C1** thus has the most extended molecular backbone of this study. It falls nevertheless close to that in the laterally functionalised molybdenum(II)-based paddle-wheel complexes of Liu and Hong.[10]

A glimpse on the molecule packing of **C1** (Figure 6) reveals a co-parallel alignment of individual molecules along the *a*-axis of the unit cell. These molecules associate by intermolecular, pairwise C–H···O contacts of 2.515 Å between acetate methyl proton H2 and oxygen atom O4 as well as weak C–H···π interactions of 2.826 Å of amine methyl proton H7 with phenyl carbon atom C10. Neighbouring chains are laterally offset along the *b*-axis of the unit cell and form pairwise C–H···O contacts of 2.577 Å between methyl proton H4A of the opposite acetate ligand to atom O3 as well as C–H···π interactions of 2.768 Å between acetate methyl proton H4 and phenyl carbon atom C12. Additional plots showing these H-bond patterns are provided in the Supporting Information.

The anilinopyrimidine bis(adduct) **C2** crystallises in the monoclinic space group *C*2/*c* with four formula units and four dichloromethane solvate molecules per unit cell. Its molecular structure (panel B in Figure 5; for an additional ORTEP see Figure S27 of the Supporting Information) exhibits great similarity with **C1**, featuring inversion symmetry and imine N–Rh bonding plus N–H···O hydrogen bonding to *trans*-disposed acetate ligands. The N2-H···O2′ interaction of 2.08 Å and the N2···O2′ distance of 2.8830(19) Å in **C2** are considerably longer than those in **C1**; the N2-H···O2′ angle of 155.0° is however similar in both complexes. With an angle of 26.35°, the plane spanned by the atoms N1=C5–N2 is somewhat tilted with respect to the Rh1–Rh1′–O1′–C1′–O2′ plane. Since the N1=C5–N2 fragment and the methylthio anchor group of **C2** are both attached to the pyrimidine unit, they reside in the same plane. Together with the much shorter distance S1···S1′ of 15.8487(8) Å, this should create a favourable situation for

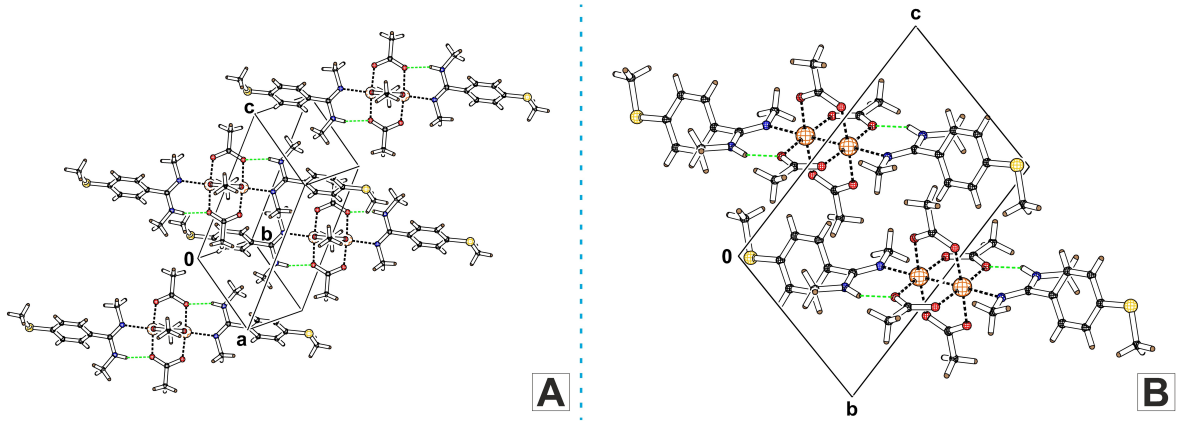

Figure 6. (**A**) Excerpt of the molecular packing of **C1** showing the intramolecular hydrogen bond-supported coordination of the axial ligand. (**B**) Top view on the *bc*-plane along the *a*-axis.

molecular charge transport. Again, the length of the Rh1–O2′ bond to the acetate oxygen donor atom involved in N–H···O hydrogen bonding of 2.0472(12) Å is longer than that of 2.0299(12) Å to its uninvolved counterpart O1. A similar discrepancy exists for the other acetate ligand, where the Rh1′–O4 bond measures 2.0475(13) Å, while the bond Rh1–O3 of 2.0339(13) Å is shorter. These differences are again caused by hydrogen bonding, this time between the oxygen atom O4 and the H atoms of the dichloromethane solvate molecule. The distance d(C–H···O) of 2.253 Å is by as much as 0.467 Å shorter than the sum of the VAN DER WAALS radii. The length of the Rh1–Rh1′ bond of 2.4013(5) Å in **C2** is shorter than that in complex **C1** and also than those in the four other entries for bis(aminopyrimidine) adducts of $Rh_2(OAc)_4$ in the CCSD database, which fall in the range of 2.409(2) Å to 2.4164(9) Å.[36]

Again, multiple intermolecular hydrogen bonding interactions generate highly ordered packing motifs in the crystal lattice. Thus, complex molecules associate into chains that run along the *c*-axis of the unit cell. Molecules within these chains have a tilt of their Rh–Rh vectors of 108.8° and are held together by the dichloromethane solvate molecules, which bridge two adjacent molecules symmetrically, as well as by weaker, pairwise C–H···O contacts of 2.664 Å between proton H2B of an acetate ligand and oxygen atom O3 of its neighbour. Parallel displaced chains of identically oriented molecules are vertically and laterally offset along the *b*- and the *c*-axes of the unit cell. Along the *b*-axis, neighbouring chains associate *via* C–H···O contacts of 2.607 Å between proton H7 of the pyrimidine ring and oxygen atom O4, C–H···S contacts of 2.922 Å between acetate methyl proton H2A and sulfur atom S1, as well as by C–H···Cl contacts of 2.844 Å between H13 at the amine-bonded phenyl ring and the dichloromethane solvate molecules. A dense network of π-stacking interactions between parallel displaced *N*-phenyl and pyrimidine rings of 3.288 Å as well as C–H···π interactions of 2.835 Å between SMe proton H9B and phenyl carbon C13 interconnect rows of molecules that are offset along the *a*-axis of the unit cell. Illustrations of the various hydrogen bond motifs are provided as Figure S28 in the Supporting Information.

In agreement with the vis data, the two isothiourea bis(adducts) **C3** and **C4** differ with respect to the identity of the axial donor atom (see Figure 7 and Figures S29 and S31 of the Supporting Information). Crystal data are provided in Table 5 and pertinent bond parameters are collected in Table 6. While the isothiourea ligand in **C3** attaches to the Rh ions *via* its imine N atom, the *N*,*N*′-diphenyl-substituted ligand **L4** prefers *κS*-coordination *via* the thioether functionality. Except for a related aminothiazole derivative, which, like **C3**, exhibits imine *κN*-coordination, complexes **C3** and **C4** seem to constitute the first isothiourea adducts of a dirhodium tetracarboxylate template to be characterised by X-ray diffraction.[37] Complexes **C3** and **C4** also exhibit intramolecular N–H···O hydrogen bonds between the amine N–H function and a carboxylate ligand (**C3**: d(N2–H···O2′) = 2.40 Å, d(N2···O2′) = 2.966(11) Å, angle N2–H···O2′ = 124.1°; **C4**: d(N2–H···O3) = 2.20 Å, d(N2···O3) = 3.039(2) Å, angle N2–H···O3 = 166.2°). With a particularly short spatial separation between the S atoms of the thioether anchor groups of only 12.069(3) Å, bis(adduct) **C3** intrinsically fulfills an important prerequisite for molecular charge transmission and is consequently a promising candidate for STM-BJ experiments.

Besides *κS*-coordination, complex **C4** has the unique feature among the present complexes that the amine N–H functionalities interact with *cis*- rather than with *trans*-disposed carboxylate ligands. This leads to a slight twisting of the central paddle-wheel core as indicated by the torsion angle O3–Rh1–Rh1′–O4 of 5.42°. Coordination *via* the prospective thioether anchor groups and steric crowding of the alternative imine binder disqualify complex **C4** for electrical contacting in STM-BJ experiments and charge transport studies. The bond length Rh1–S1 of 2.5158(7) Å falls well within the range of 2.484(3) to 2.560(2) Å found for other Rh_2(tetracarboxylate) bis(thioether) adducts, while the Rh1–Rh1′ bond of 2.3983(6) Å is unusually short when

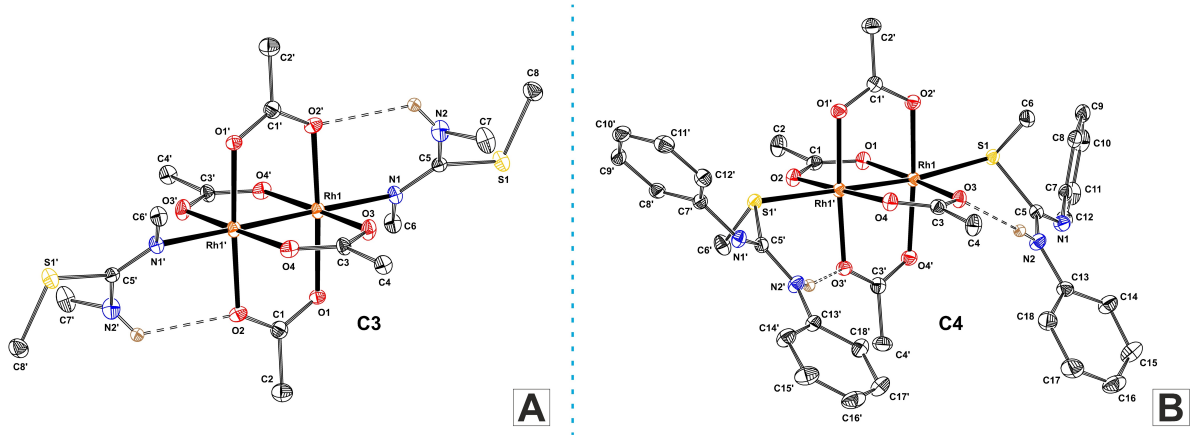

Figure 7. ORTEP of (**A**) the $Rh_2(OAc)_4$ *N*,*N*′,*S*-trimethyl-isothiourea bis(adduct) **C3** and (**B**) the *N*,*N*′-diphenyl-*S*-methyl-isothio-urea bis(adduct) **C4**. Thermal ellipsoids are displayed at a 50 % probability level. Hydrogen atoms (except for N–H) are omitted for clarity reasons.

compared to those of 2.4132(1) to 2.560(2) Å for these congeners.[38]

In the crystalline state, individual complex molecules again associate by multiple hydrogen bonding interactions. Molecules of **C3** form chains of identically oriented molecules that interconnect by pairwise C–H···O contacts between acetate protons H2A and oxygen atoms O4 of 2.636 Å along the *a*-axis, weaker C–H···π contacts of 2.838 Å between the imine carbon atom C5 and acetate proton H4C along the *b*-axis and rather strong C–H···O contacts between H8A of the SMe group and acetate oxygen O2 of 2.438 Å along the *c*-axis of the unit cell. Figure S30 of the Supporting Information provides plots of the hydrogen bond patterns in **C3**. For **C4**, equally oriented molecules form chains along the *c*-axis with pairwise, short hydrogen bonds C–H···O between acetate protons H2C and oxygen atoms O2 of 2.370 Å. These chains interact with each other along the *a*-axis by pairwise C–H···π interactions of 2.795 Å between SMe proton H6B and carbon atom C8 of the *N*-bonded phenyl ring. Additional weaker interactions C–H···O of 2.696 Å and C–H···S of 2.946 Å are established by protons H17 and H16 of the same phenyl ring and oxygen atom O1 or the thioether sulfur atom S1 along the *b*-axis of the unit cell. Figure S32 in the Supporting Information provide views of these intermolecular interactions.

DFT calculations

We next employed a DFT-based, computational approach in order to i) explore the energy differences between the two isomers that differ with respect to the mutual orientations of the carboxylate ligands that are involved in N–H···O hydrogen bonding, which is *trans* in complexes **C1**–**C3**, but *cis* in **C4**; ii) rationalise the differing preferred binding modes of the isothiourea ligands **L3** and **L4** to $Rh_2(OAc)_4$ in complexes **C3** and **C4** (κN for **L3**, but κS for **L4**); iii) provide an estimate to what extent additional N–H···O hydrogen bonding stabilises the Rh–L_{Ax} bonds; and iv) identify the most likely molecular states of complexes **C1**–**C4** that define the preferred transport channel in a STM break-junction. To these ends we geometry-optimised the *trans*- and *cis*-isomers of all complexes, including the κN- and κS-isomers of complexes **C3** and **C4**. We also considered the analogous complexes with the corresponding *N*-methylated counterparts of ligands **L1**–**L4**, henceforth denoted as **L1^{Me}**–**L4^{Me}**; they serve as points of comparison in order to assess the contribution of additional intramolecular hydrogen bonding to the acetate ligands on the axial ligand binding energy. The results of these studies are provided as Figures S33 to S60 and Tables S21 to S52 in the Supporting Information.

With respect to the mutual orientations of the acetate ligands involved in hydrogen bonding, the *trans*- and *cis*-isomers were found to be nearly isoenergetic for complexes **C1**–**C3** with an insignificant bias of 0.1 to 1.7 kJ/mol for the experimentally observed *trans*-arrangement (Table S47). However for **C4** with the κS-bonded *N*,*N*′-diphenyl-*S*-methylisothiourea ligand, the *cis*-isomer was computed to be preferred by a more substantial margin of 33.5 kJ/mol. Our calculations also reproduced the stability ordering of the κN- *and* κS-linkage isomers of complexes **C3** and **C4**. Hence, they indicate that κN-bonding is favoured by 52.5 kJ/mol for ligand **L3**, but disfavoured by 111 kJ/mol for **L4**.

In order to estimate the stabilising impact of hydrogen bonding on axial ligand binding, we subtracted the computed total Gibbs free energies *G* and the enthalpies *H* of the pristine $Rh_2(OAc)_4$ core and the corresponding uncoordinated, free ligands **L1**–**L4** from those of the bis(adducts) **C1**–**C4** and compared the results to those obtained for their congeners **C1^{Me}**–**C4^{Me}** and the *N*-methylated counterparts of **L1**–**L4**, ligands **L1^{Me}**–**L4^{Me}**. The latter are obviously incapable of forming an additional intramolecular hydrogen bond with carboxylate O donors of nearby acetate ligands. The results are provided in Tables S49 to S52 of the Supporting Information. All energy data refer to those of the corresponding geometry-optimised structures. Computed differences ΔG and ΔH range from −30 kJ/mol for **C4** to −63 kJ/mol for **C2** (ΔG),

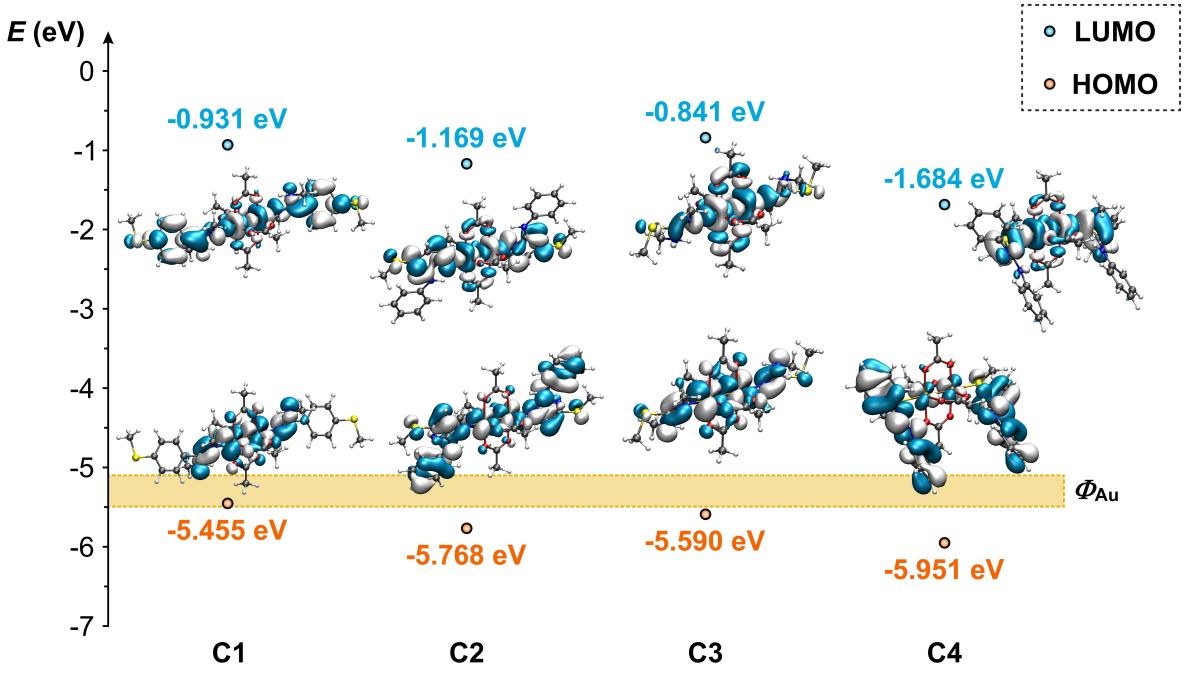

Figure 8. Energies and plots of the frontier orbitals of complexes **C1**–**C4** with respect to the typical range of the topology-dependent work function Φ of gold contacts indicated by the horizontal yellow bar ($\Phi_{Au}(100) = 5.47$ eV; $\Phi_{Au}(110) = 5.37$ eV; $\Phi_{Au}(111) = 5.31$ eV; Φ_{Au}(polycrystalline) = 5.10 eV).[39b–d] Molecular orbitals were calculated at the PBE1PBE/6-31G(d)/MWB28 level of theory and are displayed at an isosurface value of ±0.02.

or from −28 kJ/mol for **C4** to −62 kJ/mol for **C2** (ΔH). This provides us with an estimated stabilisation energy of ca. −15 to −30 kJ/mol per N–H···O hydrogen bond.

Efficient charge transport over a molecular unit requires the availability of molecular states that align favourably with the Fermi energy E_F of the electrode material, which in our STM-BJ setup is gold. In such junctions, E_F and the work function are not strictly defined and may vary from −5.53 eV to −5.10 eV, depending on the contacting crystal facet or the gold surface state.[39] As part of our pre-screening of $Rh_2(OAc)_4(L_{Ax})_2$ bis(adducts) **C1** to **C4** for STM-BJ measurements, we sought to collect additional information on the energetic alignment, delocalisation and anchor group contributions of their relevant frontier orbitals by means of quantum chemistry. All these features are essential for charge propagation and effective coupling at the metal-electrode interface. Plots of the frontier orbitals of complexes **C1**–**C4** are shown in Figure 8 and compared to the expected range of the work function of the gold contact. One should also note that hybridisation with the metallic states of gold and the ensuing level broadening will introduce shifts of frontier MO energies on the insertion of a molecule into a STM junction.

The good alignment of their HOMO with Φ_{Au}, which is nearly spot-on for **C1** and **C3**, suggests that these complexes are HOMO conductors, as it is routinely found for molecules with thiomethyl or thioether anchor groups.[40] One should note here that these considerations apply independently of the configuration of the complexes or, in the case of **C3** and **C4**, of the binding mode of the thiourea ligand. As is detailed in the Supporting Information, the energies of the frontier MOs HOMO and LUMO of *cis*- and *trans*-isomers differ only by a small margin of 0.04 eV to 0.2 eV. Energy differences for the κN- and κS-isomers are larger at 0.3 to 0.7 eV, but certainly not in a range that suffices to alter the preferred conduction channel. Moreover, complex **C4** likely disqualifies for such studies due to the binding of the prospective SMe anchor groups of ligands **L4** to the Rh ions and the steric shielding of the alternative imine donors (*vide supra*). **C1** has the disadvantageous property that the HOMO is confined to the central complex entity and the NCN benzamidine functionalities, but has no contributions from the thiomethyl-substituted phenyl rings at the amidine C atom. This is due to their pronounced tilt out of the Rh–O···H–NC5=N plane. **C1** thus does not provide a conductive pathway between both anchor groups, which adds on the unfavourably large S···S distance of this complex (*vide supra*). The remaining bis(adducts) **C2** and **C3** appear more promising as they combine a delocalised HOMO and anchor group contributions and will now be subjected to experimental studies towards their molecular conductance signatures. The results of this study will be reported in due course.

Conclusions

In the present work, we have utilised tailored, anchor group-modified RN=CR′–NHR donor ligands derived from benzamidine (ligand **L1**), anilinopyrimidine (ligand **L2**) and isothiourea

(ligands **L3** and **L4**) as axial ligands towards the $Rh_2(OAc)_4$ template. The above ligands are all capable of forming a coordinative imine N–Rh as well as a hydrogen bond to an acetate ligand of the $Rh_2(OAc)_4$ paddle-wheel motif, hence providing more robust axial coordination as compared to a simple imine donor. This was done as a possible means to make these complexes amenable to single-molecule conductance studies. Successful coordination and intramolecular hydrogen bonding were verified by NMR and IR spectroscopy as well as by single-crystal X-ray diffraction on all four complexes. ^{1}H-NMR spectroscopy revealed an increasing downfield shift of the N–*H* resonance signal from the free ligands to their corresponding complexes in the order Δ_{N-H} **C1**–**L1** > Δ_{N-H} **C4**–**L4** > Δ_{N-H} **C3**–**L3** > Δ_{N-H} **C2**–**L2**. Adduct formation is also heralded by the appearance of sharp, generally blue-shifted and highly intense N–H···O bands in their IR spectra at the expense of the broader and weaker bands for the intermolecular N–H···N′ hydrogen bonds of ligands **L1**–**L4**. The electronic spectra also showed considerable variation in the energy of the so-called A band, which corresponds to an electronic excitation from the π- to the σ-antibonding MOs within the dirhodium core, i.e. the d(π*, Rh_2)→d(σ*, Rh_2) transition. Crystallographic studies on complexes **C1**–**C4** revealed that *N*,*N*′-diphenyl-*S*-methyl-isothiourea (ligand **L4**) favours κ*S*-Rh coordination, thus binding to the metal ions through the thioether sulfur atom, whereas for the other ligands, including *N*,*N*′,*S*-trimethylisothiourea **L3**, the desired N–M + N–H···O coordination mode is realised. All complexes display intermolecular association in the crystalline state that involve C–H···O, C–H···S and C–H···π interactions as well as π-stacking interactions in complex **C2**.

Accompanying quantum chemical calculations indicate that intramolecular hydrogen bonding stabilises the Rh–L_{Ax} bond by ca. 15 kJ/mol to 30 kJ/mol. They identify these complexes as likely HOMO conductors with good energy alignment with the work function of the STM gold contacts, irrespective of whether the carboxylate ligands involved in intramolecular hydrogen bonding are *trans*- or *cis*-disposed. Based on the HOMO extension over the entire molecular backbone including the SMe anchor groups and their shorter S···S distances between the thiomethyl anchor groups, complexes **C2** and **C3** emerge as the most promising candidates among the four bis(adducts) and will now be tested in STM break-junction experiments.

Experimental Section

Synthetic procedures

If not stated otherwise, all syntheses were carried out under inert conditions by applying standard Schlenk techniques. The employed starting materials were purchased from commercial suppliers and used without further purification. Solvents were dried over appropriate drying agents, distilled and saturated with nitrogen prior to use.

NMR spectroscopy

^{1}H- and ^{13}C{^{1}H}-NMR spectra were either recorded on a Bruker Avance III 400 MHz, a Bruker Avance HD 400 MHz or a Bruker Avance III 600 MHz spectrometer applying broadband decoupling at room temperature. Data processing was performed using the Mnova software (Mestrelab Research). Chemical shifts are reported in ppm and were referenced to the peak of residual protonated solvent (^{1}H) or the solvent signal (^{13}C{^{1}H}) of the employed deuterated solvents, respectively. Coupling constants are reported in Hertz (Hz).

Elemental analysis

Elemental analysis was carried out using an UNICUBE (unicu-CHNS-120) organic elemental analyser from Elementar. Due to the general interference of fluorine-containing samples with the high combustion temperature necessary for the determination of sulfur contents, only the CHN shares of the reported compounds were analysed.

HR-ESI-MS

High-resolution mass spectra were recorded on a LTQ Orbitrap Velos spectrometer from Thermo Fisher Scientific (Velos Pro) with or without loop-mode injection from a Waters (RP18) HPLC system. Ionisation was achieved by the electrospray ionisation (ESI) technique. Detection was done in the positive-ion mode using dichloromethane as the sample solvent.

X-ray diffraction analysis

Single crystals of ligand **L1** were obtained by slow evaporation of a dichloromethane solution of this compound, while those of **C1**–**C4** were grown by layer diffusion of *n*-pentane into dichloromethane solutions of the respective complexes. X-ray diffraction analysis was conducted on a STOE IPDS II diffractometer equipped with a graphite-monochromated Mo-K_α ($\lambda = 0.71073$ Å) radiation source and an image plate detection system at $T = 100$ K. Data processing was carried out with X-Area software (STOE). Structure solution was accomplished by employing Olex2[41] in combination with the SHELXT[42] program. Further refinement was performed using the SHELXL package.[43] Hydrogen atoms were introduced at their calculated positions. Evaluation of the CIF-files was carried out and crystal packing representations were rendered with Mercury.[44] ORTEPs were generated with Platon.[45]

IR spectroscopy

Infrared spectra of all compounds were recorded either in form of KBr pellets or in dichloromethane solution on a Bruker Tensor II FT-IR spectrometer. Data processing was conducted with the corresponding OPUS software (Bruker).

UV/vis spectroscopy

Electronic absorption spectra of all complexes were acquired in dichloromethane solution at r.t. in Hellma quartz cuvettes with an optical path length of 0.2 cm using a TIDAS S MCS UV/NIR spectrometer from J&M Analytik AG.

Quantum Chemistry

Electronic ground-state structures were calculated by density functional theory methods employing the Gaussian16[46] program package. Quantum-chemical studies were performed without symmetry constraints. The polarised double-ζ basis set 6-31G(d)[47] in combination with the Perdew-Burke-Ernzerhof exchange and correlation functional PBE1PBE[48] was employed for main group elements. For rhodium, quasi-relativistic Wood-Boring small-core pseudopotentials[49] with the corresponding optimised set of basis functions (MWB28)[50] were applied. Geometry optimisations and consecutive vibrational analyses were performed in solvent media by employing the polarisable continuum model (PCM)[51] with the standard parameters for dichloromethane. Vibrational data were corrected for their offset in zero-point energies with the vibrational frequency scaling factor of 0.9512 as recommended for PBE1PBE/6-31G(d) combination of functional and basis set functions.[25] The calculated IR data was extracted and processed using GaussSum.[52]

Synthesis and Characterisation

4-(Methylthio)benzoyl chloride (2)[53]

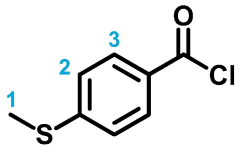

Thionyl chloride (30 mL, 49.2 g, 413.55 mmol, 6.96 eq.) was added to 4-methylthiobenzoic acid (10.0 g, 59.45 mmol, 1.00 eq.) under ambient conditions and the resulting suspension was heated at reflux until the gas evolution subsided (3 h). After cooling to r.t., excess thionyl chloride was distilled off under ambient pressure and the obtained viscous oil was dried *in vacuo* affording the title compound as a yellow solid in quantitative yield (11.1 g, 59.45 mmol). Compound **2** was used in the consecutive synthesis step without further purification.

^{1}H-NMR (400 MHz, $CDCl_3$): δ (ppm) = 7.99 (d, $^3J_{HH}$ = 8.64 Hz, 2H, *H*-3), 7.28 (d, $^3J_{HH}$ = 8.64 Hz, 2H, *H*-2), 2.54 (s, 3H, *H*-1).

N-Methyl-4-(methylthio)benzamide (3)[53]

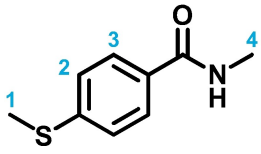

4-(Methylthio)benzoyl chloride (**2**) (8.19 g, 43.88 mmol, 1.00 eq.) was added portionwise at 0 °C to methylammonium chloride (4.44 g, 65.82 mmol, 1.50 eq.) and potassium carbonate (12.13 g, 87.76 mmol, 2.00 eq.), dissolved in a mixture of ethyl acetate and deionised water (150 mL, 2 : 1 *v*/*v*). The resulting biphasic reaction mixture was stirred at 0 °C for 1 h before it was allowed to reach r.t. Stirring was continued for another 6 h. A white precipitate formed and was isolated by filtration and dried under reduced pressure. The filtrate was phase-separated in a separation funnel and the organic phase was washed with deionised water (2 × 50 mL), dried over magnesium sulfate and the solvent was removed *in vacuo*. The obtained white solid and the isolated precipitate were combined and recrystallised from a mixture of acetone and *n*-heptane (1 : 3, *v*/*v*), furnishing compound **3** as white solid in 92% yield (7.35 g, 40.55 mol).

^{1}H-NMR (400 MHz, $CDCl_3$): δ (ppm) = 7.67 (d, $^3J_{HH}$ = 8.42 Hz, 2H, *H*-3), 7.25 (d, $^3J_{HH}$ = 8.42 Hz, 2H, *H*-2), 6.13 (s, 1H, N–*H*), 3.00 (d, $^3J_{HH}$ = 4.85 Hz, 3H, *H*-4), 2.50 (s, 3H, *H*-1).

N-Methyl-4-(methylthio)benzimidoyl chloride (4)

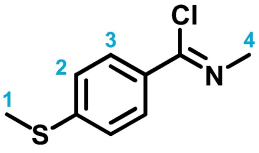

N-Methyl-4-(methylthio)benzamide (**2**) (6.91 g, 38.12 mmol, 1.00 eq.) was dissolved in thionyl chloride (12.5 mL, 20.5 g, 172.31 mmol, 4.52 eq.) and the resulting solution was heated at reflux until the gas evolution subsided (4 h). After cooling to r.t., excess thionyl chloride was distilled off under ambient pressure and the viscous, orange oil was dried *in vacuo*. The crude product was purified *via* distillation under reduced pressure (103 °C at 1.5 × 10^{-2} mbar). Compound **4** was isolated as yellow oil in 76% yield (5.79 g, 28.99 mmol) and was used in the consecutive conversion without further purification.

^{1}H-NMR (400 MHz, $CDCl_3$): δ (ppm) = 8.01 (d, $^3J_{HH}$ = 8.38 Hz, 2H, *H*-3), 7.25 (d, $^3J_{HH}$ = 8.38 Hz, 2H, *H*-2), 3.49 (s, 3H, *H*-4), 2.50 (s, 3H, *H*-1).

N,N′-Dimethyl-4-(methylthio)benzamidine (L1)[15]

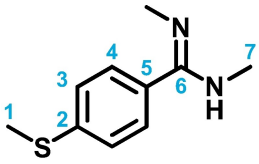

N-Methyl-4-(methylthio)benzimidoyl chloride (**4**) (5.50 g, 27.54 mmol, 1.00 eq.) was added dropwise at 0 °C to a cooled solution of methylammonium chloride (5.58 g, 82.62 mmol, 3.00 eq.) and sodium hydroxide (3.30 g, 86.62 mmol, 3.00 eq.) in deionised water (100 mL). The reaction mixture was stirred for 1 h at 0 °C before it was allowed to reach r.t., where stirring was continued for another 16 h. The aqueous mixture was extracted with dichloromethane (3 × 50 mL) and the layers were separated. The combined organic phase was treated with aqueous hydrochloric acid (1 M, 100 mL) and the layers were separated. The bright yellow aqueous phase was brought to pH = 14 by the addition of an aqueous sodium hydroxide solution (1 M), which caused the precipitation of a white solid. The mixture was extracted with dichloromethane (3 × 50 mL), dried over sodium sulfate and the solvent was removed under reduced pressure. The crude product was recrystallised from acetone, affording the title compound **L1** as colourless crystals in 27% yield (1.47 g, 7.57 mmol).

^{1}H-NMR (400 MHz, CD_2Cl_2) δ (ppm) = 7.26 (d, $^3J_{HH}$ = 8.45 Hz, 2H, *H*-3), 7.19 (d, $^3J_{HH}$ = 8.45 Hz, 2H, *H*-4), 4.11 (s, 1H, N–*H*), 2.83 (s, 6H, *H*-7), 2.49 (s, 3H, *H*-1).

^{13}C{^{1}H}-NMR (101 MHz, CD_2Cl_2) δ (ppm) = 160.4 (s, *C*-6), 140.2 (s, *C*-2), 132.7 (s, *C*-5), 128.7 (s, *C*-4), 126.4 (s, *C*-3), 15.8 (s, *C*-1).

ESI-MS $[C_{10}H_{15}N_2S]^+$ m/z (relative intensity %): calcd.: 195.0951 (100), 196.0984 (10.8), 197.0909 (4.5); found: 195.0947 (100), 196.0982 (11.2), 197.0906 (4.9).

2-Chloro-4-(methylthio)pyrimidine (6)[16]

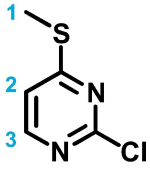

A suspension of sodium methanethiolate (1.26 g, 17.94 mmol, 1.10 eq.) in dry *N*,*N*-dimethylformamide (80 mL) was added portion-wise at 0 °C to a cooled solution of 2,4-dichloropyrimidine (**5**) (2.43 g, 16.31 mmol, 1.00 eq.) in dry *N*,*N*-dimethylformamide (60 mL). The reaction mixture was stirred for 1 h before it was allowed to reach r.t., where stirring was continued for another 16 h. The solvent was removed under reduced pressure and diethyl ether (100 mL) was added to the oily residue. The organic layer was washed with deionised water (2×50 mL), dried over sodium sulfate and the volatiles were removed *in vacuo*. The crude product was purified *via* column chromatography over silica using a mixture of *n*-pentane and ethyl acetate (4:1, *v*/*v*) as eluent. Recrystallisation from *n*-heptane gave compound **6** as colourless, low melting crystals in 34% yield (0.91 g, 5.67 mmol).

^{1}H-NMR (400 MHz, $CDCl_3$): δ (ppm) = 8.19 (d, $^3J_{HH}$ = 5.45 Hz, 1H, *H*-3), 7.09 (d, $^3J_{HH}$ = 5.45 Hz, 1H, *H*-2), 2.57 (s, 3H, *H*-1).

4-(Methylthio)-N-phenylpyrimidine-2-amine (L2)

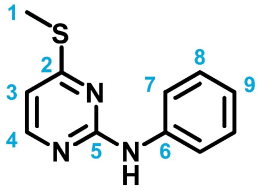

2-Chloro-4-(methylthio)pyrimidine (**6**)[16] (400 mg, 2.49 mmol, 1.00 eq.) was dissolved in aniline (0.46 mL, 469 mg, 5.04 mmol, 2.02 eq.) and the resulting solution was heated to 120 °C for 2 h. After cooling to r.t., the yellow residue was extracted with dichloro-methane (30 mL). The organic layer was washed with saturated aqueous sodium hydrogencarbonate solution (2×20 mL) and dried over magnesium sulfate. Removal of the solvent under reduced pressure gave the crude product as a colourless oil, which solidified on standing at r.t. Recrystallisation from *n*-heptane at −18 °C afforded **L2** as colourless crystals in 82% yield (443 mg, 2.04 mmol).

^{1}H-NMR (400 MHz, CD_2Cl_2) δ (ppm) = 8.07 (d, $^3J_{HH}$ = 5.39 Hz, 1H, *H*-4), 7.65 (dd, $^3J_{HH}$ = 8.54 Hz, $^4J_{HH}$ = 1.11 Hz, 2H, *H*-7), 7.60 (s, 1H, N–*H*), 7.33 (dd, $^3J_{HH}$ = 8.54 Hz, $^3J_{HH}$ = 7.38 Hz, 2H, *H*-8), 7.04 (tt, $^3J_{HH}$ = 7.38 Hz, $^4J_{HH}$ = 1.11 Hz, 1H, *H*-9), 6.65 (d, 1H, $^3J_{HH}$ = 5.39 Hz, 1H, *H*-3), 2.55 (s, 3H, *H*-1).

^{13}C{^{1}H}-NMR (101 MHz, CD_2Cl_2) δ (ppm) = 171.8 (s, *C*-2), 160.0 (s, *C*-5), 155.9 (s, *C*-4), 140.2 (s, *C*-6), 129.3 (s, *C*-8), 122.9 (s, *C*-9), 119.9 (s, *C*-7), 110.3 (s, *C*-3), 13.0 (s, *C*-1).

ESI-MS $[C_{11}H_{12}N_3S]^+$ m/z (relative intensity %) = calcd.: 218.0747 (100), 219.0780 (11.9), 220.0705 (4.5), 219.0717 (1.1); found: 218.0740 (100), 219.0775 (12.3), 220.0707 (4.8), 219.0714 (0.7).

General procedure for the synthesis of N,N′,S-trimethylisothiourea (L3) and N,N′-diphenyl-S-methylisothiourea (L4)[17]

Preparation of the hydroiodides **8** and **10**

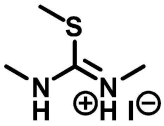

8

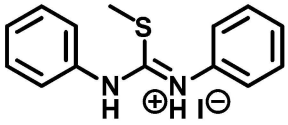

10

N,*N*′-Dimethylthiourea (**7**) (10.0 g, 96.00 mmol, 1.00 eq.) or *N*,*N*′-diphenylthiourea (**9**) (10.0 g, 43.80 mmol, 1.00 eq.) was dissolved in a minimum amount of acetone (**7**: 25 mL; **9**: 200 mL). Methyl iodide (**7**: 6.0 mL, 13.6 g, 96.00 mmol, 1.00 eq; **9**: 2.7 mL, 6.2 g, 43.80 mmol, 1.00 eq.) was added dropwise to the vigorously stirred solution at r.t. Stirring was continued for 16 h. The solvent was removed under reduced pressure and the obtained product was washed with diethyl ether (3×20 mL) and dried *in vacuo*, yielding the respective isothiourea hydroiodide as white solid in 76% yield (**8**: 18.1 g, 73.54 mmol) or 84% yield (**10**: 13.7 g, 37.00 mmol).

Preparation of **L3** and **L4**:

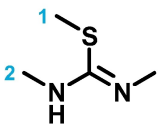

L3

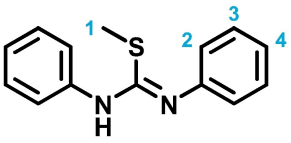

L4

An aqueous solution of compound **8** (16.9 g, 68.67 mmol, 1.00 eq. in 350 mL deionised water) or an aqueous suspension of compound **10** (8.0 g, 21.61 mmol, 1.00 eq. in 250 mL deionised water) was cooled to 0 °C in an ice bath and brought to pH = 14 by slow addition of concentrated aqueous ammonia. The mixture was allowed to reach r.t. and then stirred for 1 h. The aqueous phase was extracted with dichloromethane (2×100 mL) and the layers were separated. The combined organic phases were dried over sodium sulfate and the solvent was removed under reduced pressure. Recrystallisation from *n*-heptane gave the respective isothiourea ligand **L3** or **L4** as white crystals.

L3: 50% (4.1 g, 34.69 mmol).

^{1}H-NMR (400 MHz, $CDCl_3$): δ (ppm) = 3.84 (s, 1H, N–*H*), 2.95 (s, 6H, *H*-2), 2.37 (s, 3H, *H*-1).

L4: 97% (5.1 g, 21.04 mmol).

^{1}H-NMR (400 MHz, $CDCl_3$): δ (ppm) = 7.32 (dd, $^3J_{HH}$ = 7.59 Hz, $^3J_{HH}$ = 7.38 Hz, 4H, *H*-3), 7.20 (d, $^3J_{HH}$ = 7.59 Hz, 4H, *H*-2), 7.09 (t, $^3J_{HH}$ = 7.38 Hz, 2H, *H*-4), 6.16 (s, 1H, N–*H*), 2.31 (s, 3H, *H*-1).

ESI-MS $[C_{14}H_{15}N_2S]^+$ m/z (relative intensity %) = calcd.: 243.0951 (100), 244.0984 (15.1), 245.0909 (4.5), 245.1018 (1.1); found: 243.0949 (100), 244.0975 (15.0), 245.0903 (4.7), 245.1005 (1.0).

General procedure for the synthesis of rhodium(II) acetate bis(adducts) C1-C4

Dirhodium(II) tetraacetate **11** (87.0 mg, 196.84 mmol, 1.00 eq.) was generated by carefully heating $Rh_2OAc_4 \cdot 2$ MeOH (100.0 mg, 196.84 mmol, 1.00 eq.) under reduced pressure until the colour had

changed from dark blue to emerald green. The respective ligand (**L1**: 76.5 mg; **L2**: 85.5 mg; **L3**: 46.5 mg; **L4**: 95.4 mg, 393.68 mmol, 2.00 eq.) was added, the mixture was dissolved in dry dichloromethane (5 mL) and stirred at r.t. for 1 h. The solution was filtered, layered with *n*-pentane and left to stand. After several days, crystals of **C1**–**C4** were obtained.

C1: 78% (127.5 mg, 153.54 mmol). **^{1}H-NMR** (400 MHz, CD_2Cl_2): δ (ppm) = 7.51 (bm, 8H, *H*-2, *H*-3), 6.49 (bs, 2H, N–*H*), 3.34 (bs, 6H, *H*-4/*H*-4′), 2.62 (bs, 12H, *H*-4/*H*-4′, *H*-1), 1.86 (s, 12H, *H*-5). The assignment *H*-X/*H*-X′ corresponds to either of the indicated nuclei.

Elemental analysis $[C_{28}H_{40}N_4O_8Rh_2S_2]$: calcd.: C, 40.49; H, 4.85; N, 6.75; found: C, 40.30; H, 4.96; N, 6.83.

ESI-MS $[C_{28}H_{40}N_4O_8Rh_2S_2]^+$ m/z (relative intensity %): calcd. 830.0393 (100), 831.0426 (30.3), 832.0351 (9.0); found: 830.0422 (100), 831.0460 (44.5), 832.0606 (9.3).

C2×CH$_2$Cl$_2$: 49% (93.2 mg, 96.93 mmol). **^{1}H-NMR** (400 MHz, CD_2Cl_2): δ (ppm) = 9.02 (s, 2H, N–*H*), 8.54 (d, $^3J_{HH}$ = 5.84 Hz, 2H, *H*-3), 7.68 (dd, $^3J_{HH}$ = 8.60 Hz, $^4J_{HH}$ = 1.10 Hz, 4H, *H*-4), 7.36 (dd, $^3J_{HH}$ = 8.60 Hz, $^3J_{HH}$ = 7.37 Hz, 4H, *H*-5), 7.08 (tt, $^3J_{HH}$ = 7.37 Hz, $^4J_{HH}$ = 1.10 Hz, 2H, *H*-6), 6.96 (d, $^3J_{HH}$ = 5.84 Hz, 2H, *H*-2), 2.71 (s, 6H, *H*-1), 1.92 (s, 12H, *H*-7).

Elemental analysis $[C_{31}H_{36}Cl_2N_6O_8Rh_2S_2]$ for **C2×CH$_2$Cl$_2$**: calcd.: C, 38.73; H, 3.77; N, 8.74; found: C, 39.06; H, 4.24; N, 9.13.

ESI-MS Superposition of $[C_{30}H_{34}N_6O_8Rh_2S_2]^+$ and $[C_{30}H_{34}N_6O_8Rh_2S_2]+H^+$ m/z (relative intensity %): calcd. 877.0063 (100), 878.0096 (32.4), 875.9990 (M^+), 879.0021 (9.0); found: 877.0046 (100), 875.9949 (M^+, 28.1), 878.0063 (20.5), 879.0195 (2.2).

C3: 46% (61.4 mg, 90.55 mmol). **^{1}H-NMR** (400 MHz, CD_2Cl_2): δ (ppm) = 5.82 (s, 2H, N–*H*), 3.59 (s, 6H, *H*-2), 2.91 (s, 6H, *H*-2′), 2.58 (s, 6H, *H*-1), 1.85 (s, 12H, *H*-3).

Elemental analysis $[C_{16}H_{32}N_4O_8Rh_2S_2]$: calcd.: C, 28.33; H, 4.75; N, 8.26; found: C, 28.14; H, 4.85; N, 7.66.

ESI-MS Superposition of $[C_{16}H_{32}N_4O_8Rh_2S_2]^+$ and $[C_{16}H_{32}N_4O_8Rh_2S_2]+H^+$ m/z (relative intensity %): calcd. 678.9845 (100), 677.9772 (M^+), 679.9878 (17.3), 680.9803 (9.0); found: 678.9878 (100), 677.9796 (M^+, 87.9), 680.9773 (16.5), 679.9915 (7.4).

C4: 80% (145.9 mg, 157.47 mmol). **^{1}H-NMR** (400 MHz, CD_2Cl_2): δ (ppm) = 8.17 (s, 2H, N–*H*), 7.60–6.95 (bm, 20H, *H*-Aryl), 2.46 (s, 6H, *H*-1), 1.79 (s, 12H, *H*-2).

Elemental analysis $[C_{36}H_{40}N_4O_8Rh_2S_2]$: calcd.: C, 46.66; H, 4.35; N, 6.05; found: C, 45.97; H, 4.57; N, 6.05.

ESI-MS $[C_{36}H_{40}N_4O_8Rh_2S_2]+H^+$ m/z (relative intensity %): calcd. 927.0471 (100), 928.0504 (38.9), 929.0429 (9.0); found: 927.0437 (100).

Acknowledgements

We thank the State of Baden-Württemberg for providing us with resources and the computational facilities of the Scientific Computing Center SCC of the University of Konstanz. Open Access funding enabled and organized by Projekt DEAL.

Conflict of Interest

The authors declare no conflict of interest.

Data Availability Statement

The data that support the findings of this study are available in the Supporting Information to this article. CCDC numbers 2175012 (**L1**), 2175013 (**C1**), 2175016 (**C2**), 2175014 (**C3**) and 2175015 (**C4**) contain the crystallographic information for the compounds featured in this paper. The data can be obtained free of charge *via* https://www.ccdc.cam.ac.uk/structures/ or by contacting The Cambridge Crystallographic Data Centre (12 Union Road, Cambridge, CB2 1EZ, United Kingdom).

Keywords: Hydrogen bonds · Paddle-wheel complexes · Rhodium · Crystal structures · DFT-calculations

[1] a) J. N. van Niekerk, F. R. L. Schoening, J. F. de Wet, *Acta Crystallogr.* **1953**, *6*, 501–504; b) J. N. van Niekerk, F. R. L. Schoening, *Nature* **1953**, *171*, 36–37; c) J. N. van Niekerk, F. R. L. Schoening, *Acta Crystallogr.* **1953**, *6*, 227–232.
[2] F. A. Cotton, B. G. DeBoer, M. D. Laprade, J. R. Pipal, D. A. Ucko, *J. Am. Chem. Soc.* **1970**, *92*, 2926–2927.
[3] D. Lawton, R. Mason, *J. Am. Chem. Soc.* **1965**, *87*, 921–922.
[4] F. A. Cotton, *Inorg. Chem.* **1965**, *4*, 334–336.
[5] a) F. A. Cotton, E. A. Hillard, C. A. Murillo, H.-C. Zhou, *J. Am. Chem. Soc.* **2000**, *122*, 416–417; b) F. A. Cotton, L. R. Falvello, A. H. Reid Jnr, W. J. Roth, *Acta Crystallogr. Sect. C* **1990**, *46*, 1815–1818; c) F. A. Cotton, J. G. Norman, *J. Coord. Chem.* **1972**, *1*, 161–171.
[6] a) S. Ogawa, S. Chattopadhyay, Y. Tanaka, T. Ohto, T. Tada, H. Tada, S. Fujii, T. Nishino, M. Akita, *Chem. Sci.* **2021**, *12*, 10871–10877; b) F. A. Cotton, C. Y. Liu, C. A. Murillo, *Inorg. Chem.* **2004**, *43*, 2267–2276; c) J. L. Bear, B. Han, S. Huang, K. M. Kadish, *Inorg. Chem.* **1996**, *35*, 3012–3021; d) J. L. Bear, B. Han, S. Huang, *J. Am. Chem. Soc.* **1993**, *115*, 1175–1177.
[7] a) A. Raghavan, T. Ren, *Organometallics* **2019**, *38*, 3888–3896; b) G. Xu, C. Campana, T. Ren, *Inorg. Chem.* **2002**, *41*, 3521–3527; c) A. Bino, F. A. Cotton, W. Kaim, *Inorg. Chem.* **1979**, *18*, 3566–3568.
[8] a) A. Raghavan, B. L. Mash, T. Ren, *Inorg. Chem.* **2019**, *58*, 2618–2626; b) B. Xi, G. L. Xu, J. W. Ying, H. L. Han, A. Cordova, T. Ren, *J. Organomet. Chem.* **2008**, *693*, 1656–1663; c) A. K. Mahapatro, J. Ying, T. Ren, D. B. Janes, *Nano Lett.* **2008**, *8*, 2131–2136; d) A. S. Blum, T. Ren, D. A. Parish, S. A. Trammell, M. H. Moore, J. G. Kushmerick, G. L. Xu, J. R. Deschamps, S. K. Pollack, R. Shashidhar, *J. Am. Chem. Soc.* **2005**, *127*, 10010–10011; e) K. M. Kadish, T. D. Phan, L. Giribabu, E. Van Caemelbecke, J. L. Bear, *Inorg. Chem.* **2003**, *42*, 8663–8673; f) A. R. Chakravarty, F. A. Cotton, D. A. Tocher, *Inorg. Chem.* **1985**, *24*, 172–177; g) A. R. Chakravarty, F. A. Cotton, E. S. Shamshoum, *Inorg. Chem.* **1984**, *23*, 4216–4221.
[9] a) F. A. Cotton, Z. Li, C. A. Murillo, *Eur. J. Inorg. Chem.* **2007**, *2007*, 3509–3513; b) F. A. Cotton, C. A. Murillo, R. Yu, *Dalton Trans.* **2006**, 3900–3905; c) J. F. Berry, F. A. Cotton, S. A. Ibragimov, C. A. Murillo, X. Wang, *Dalton Trans.* **2003**, 4297–4302; d) F. A. Cotton, L. M. Daniels, C. Lin, C. A. Murillo, *J. Am. Chem. Soc.* **1999**, *121*, 4538–4539.
[10] M. Meng, Z. Tang, S. Mallick, M. H. Luo, Z. Tan, J. Y. Liu, J. Shi, Y. Yang, C. Y. Liu, W. Hong, *Nanoscale* **2020**, *12*, 10320–10327.
[11] a) D. Bu, Y. Xiong, Y. N. Tan, M. Meng, P. J. Low, D. B. Kuang, C. Y. Liu, *Chem. Sci.* **2018**, *9*, 3438–3450; b) D. Bu, Y. Xiong, Y. N. Tan, M. Meng, C. Y. Liu, *Chem. Commun.* **2018**, *54*, 3632–3635.
[12] H. E. Skipper, C. V. May, A. L. Rheingold, L. H. Doerrer, M. Kamenetska, *J. Am. Chem. Soc.* **2021**, *143*, 16439–16447.

[13] a) L. Wang, Z. L. Gong, S. Y. Li, W. Hong, Y. W. Zhong, D. Wang, L. J. Wan, *Angew. Chem. Int. Ed.* **2016**, *55*, 12393–12397; *Angew. Chem.* **2016**, *128*, 12581–12585; b) X. Chen, *J. Biol. Phys.* **2013**, *39*, 607–624; c) M. Wimmer, J. L. Palma, P. Tarakeshwar, V. Mujica, *J. Phys. Chem. Lett.* **2016**, *7*, 2977–2980; d) T. Nishino, N. Hayashi, P. T. Bui, *J. Am. Chem. Soc.* **2013**, *135*, 4592–4595.
[14] a) Y. S. Park, A. C. Whalley, M. Kamenetska, M. L. Steigerwald, M. S. Hybertsen, C. Nuckolls, L. Venkataraman, *J. Am. Chem. Soc.* **2007**, *129*, 15768–15769; b) H. Vazquez, R. Skouta, S. Schneebeli, M. Kamenetska, R. Breslow, L. Venkataraman, M. S. Hybertsen, *Nat. Nanotechnol.* **2012**, *7*, 663–667.
[15] a) Y. Q. Yuan, P. S. Kumar, C. N. Zhang, M. H. Yang, S. R. Guo, *Org. Biomol. Chem.* **2017**, *15*, 7330–7338; b) M. Keenan, M. J. Abbott, P. W. Alexander, T. Armstrong, W. M. Best, B. Berven, A. Botero, J. H. Chaplin, S. A. Charman, E. Chatelain, T. W. von Geldern, M. Kerfoot, A. Khong, T. Nguyen, J. D. McManus, J. Morizzi, E. Ryan, I. Scandale, R. A. Thompson, S. Z. Wang, K. L. White, *J. Med. Chem.* **2012**, *55*, 4189–4204; c) W.-Z. Chen, G.-L. Xu, C. G. Jablonski, T. Ren, *J. Mol. Struct.* **2008**, *890*, 90–94.
[16] S. M. Smith, S. L. Buchwald, *Org. Lett.* **2016**, *18*, 2180–2183.
[17] V. I. Cohen, *Synthesis* **1980**, *1980*, 60–63.
[18] a) F. A. Cotton, T. R. Felthouse, S. Klein, *Inorg. Chem.* **1981**, *20*, 3037–3042; b) C. T. Eagle, D. G. Farrar, C. U. Pfaff, J. A. Davies, C. Kluwe, L. Miller, *Organometallics* **1998**, *17*, 4523–4526; c) S. A. Johnson, H. R. Hunt, H. M. Neumann, *Inorg. Chem.* **1963**, *2*, 960–962.
[19] a) D. Lin-Vien, N. B. Colthup, W. G. Fateley, J. G. Grasselli, *The Handbook of Infrared and Raman Characteristic Frequencies of Organic Molecules*, Academic Press, San Diego **1991**; b) T. Fornaro, D. Burini, M. Biczysko, V. Barone, *J. Phys. Chem. A* **2015**, *119*, 4224–4236.
[20] Y. S. Kara, S. G. Sagdinc, N. Karadayi, *Spectrochim. Acta Part A* **2013**, *110*, 351–363.
[21] E. D. Raczyńska, C. Laurence, M. Berthelot, *Analyst* **1994**, *119*, 683–687.
[22] N. W. Alcock, N. C. Blacker, W. Errington, M. G. H. Wallbridge, J. Barker, *Acta Crystallogr. Sect. C* **1994**, *50*, 456–458.
[23] A. J. Bortoluzzi, A. Echevarria, C. E. Rodrigues-Santos, *Acta Crystallogr. Sect. E* **2004**, *60*, O1837–O1839.
[24] J. I. Clodt, C. Wigbers, R. Reiermann, R. Frohlich, E. U. Wurthwein, *Eur. J. Org. Chem.* **2011**, *2011*, 3197–3209.
[25] J. P. Merrick, D. Moran, L. Radom, *J. Phys. Chem. A* **2007**, *111*, 11683–11700.
[26] a) V. M. Miskowski, W. P. Schaefer, B. S. Sadeghi, B. D. Santarsiero, H. B. Gray, *Inorg. Chem.* **1984**, *23*, 1154–1162; b) J. W. Trexler, A. F. Schreiner, F. A. Cotton, *Inorg. Chem.* **1988**, *27*, 3265–3267.
[27] E. Warzecha, T. C. Berto, C. C. Wilkinson, J. F. Berry, *J. Chem. Educ.* **2019**, *96*, 571–576.
[28] Y. Kataoka, Y. Kitagawa, T. Saito, Y. Nakanishi, K. Sato, Y. Miyazaki, T. Kawakami, M. Okumura, W. Mori, K. Yamaguchi, *Supramol. Chem.* **2011**, *23*, 329–336.
[29] J. D. Korp, I. Bernal, *Chem. Scr.* **1983**, *22*, 60–63.
[30] a) B. Tinant, J. Dupont-Fenfau, J.-P. Declercq, J. Podlaha, O. Exner, *Collect. Czech. Chem. Commun.* **1989**, *54*, 3245–3252; b) W. Chen, T. Ren, *J. Cluster Sci.* **2007**, *19*, 99–108.
[31] F. Nicolò, G. Bruno, S. Lo Schiavo, M. S. Sinicropi, P. Piraino, *Inorg. Chim. Acta* **1994**, *223*, 145–149.
[32] N. Farrell, M. D. Vargas, Y. A. Mascarenhas, M. T. D. Gambardella, *Inorg. Chem.* **1987**, *26*, 1426–1429.
[33] D. Pogozhev, S. A. Baudron, M. W. Hosseini, *Dalton Trans.* **2011**, *40*, 7403–7411.
[34] J. F. Berry, F. A. Cotton, C. Lin, C. A. Murillo, *J. Cluster Sci.* **2004**, *15*, 531–541.
[35] H. T. Chifotides, K. R. Dunbar, J. H. Matonic, N. Katsaros, *Inorg. Chem.* **1992**, *31*, 4628–4634.
[36] a) M. A. Zoroddu, L. Naldini, F. Demartin, N. Masciocchi, *Inorg. Chim. Acta* **1987**, *128*, 179–183; b) K. Aoki, H. Yamazaki, *Acta Crystallogr. Sect. C* **1989**, *45*, 730–734.
[37] M. Selkti, A. Tomas, B. Viossat, G. Baziard-Mouysset, T. Prangé, *Z. Kristallogr. New Cryst. Struct.* **1997**, *212*, 337–338.
[38] a) F. A. Cotton, T. R. Felthouse, *Inorg. Chem.* **1980**, *19*, 323–328; b) V. Brunskill, A. Enriquez Garcia, F. Jalilehvand, B. S. Gelfand, M. Wu, *J. Coord. Chem.* **2019**, *72*, 2177–2188; c) R. J. H. Clark, A. J. Hempleman, H. M. Dawes, M. B. Hursthouse, C. D. Flint, *J. Chem. Soc. Dalton Trans.* **1985**, 1775–1780; d) G. Matsubayashi, K. Yokoyama, T. Tanaka, *J. Chem. Soc. Dalton Trans.* **1988**, 3059–3062.
[39] a) J. C. Cuevas, E. Scheer, *Molecular Electronics: An Introduction to Theory and Experiment, Vol. Volume 1*, World Scientific **2010**; b) J. R. Rumble, *Handbook of Chemistry and Physics*, 101 ed., CRC Press, Boca Raton, Florida US **2020**; c) D. E. Eastman, *Phys. Rev. B* **1970**, *2*, 1–2; d) H. B. Michaelson, *J. Appl. Phys.* **1977**, *48*, 4729–4733.
[40] a) S. Martin, I. Grace, M. R. Bryce, C. Wang, R. Jitchati, A. S. Batsanov, S. J. Higgins, C. J. Lambert, R. J. Nichols, *J. Am. Chem. Soc.* **2010**, *132*, 9157–9164; b) V. Kaliginedi, P. Moreno-Garcia, H. Valkenier, W. Hong, V. M. Garcia-Suarez, P. Buiter, J. L. Otten, J. C. Hummelen, C. J. Lambert, T. Wandlowski, *J. Am. Chem. Soc.* **2012**, *134*, 5262–5275; c) P. Moreno-Garcia, M. Gulcur, D. Z. Manrique, T. Pope, W. Hong, V. Kaliginedi, C. Huang, A. S. Batsanov, M. R. Bryce, C. Lambert, T. Wandlowski, *J. Am. Chem. Soc.* **2013**, *135*, 12228–12240; d) C. Huang, A. V. Rudnev, W. Hong, T. Wandlowski, *Chem. Soc. Rev.* **2015**, *44*, 889–901; e) T. A. Su, M. Neupane, M. L. Steigerwald, L. Venkataraman, C. Nuckolls, *Nat. Rev. Mater.* **2016**, *1*, 16002; f) S. Gunasekaran, D. Hernangomez-Perez, I. Davydenko, S. Marder, F. Evers, L. Venkataraman, *Nano Lett.* **2018**, *18*, 6387–6391; g) S. Ogawa, S. Chattopadhyay, Y. Tanaka, T. Ohto, T. Tada, H. Tada, S. Fujii, T. Nishino, M. Akita, *Chem. Sci.* **2021**, *12*, 10871–10877.
[41] O. V. Dolomanov, L. J. Bourhis, R. J. Gildea, J. A. K. Howard, H. Puschmann, *J. Appl. Crystallogr.* **2009**, *42*, 339–341.
[42] G. M. Sheldrick, *Acta Crystallogr. Sect. A* **2015**, *71*, 3–8.
[43] G. M. Sheldrick, *Acta Crystallogr. Sect. C* **2015**, *71*, 3–8.
[44] a) C. F. Macrae, P. R. Edgington, P. McCabe, E. Pidcock, G. P. Shields, R. Taylor, M. Towler, J. van de Streek, *J. Appl. Crystallogr.* **2006**, *39*, 453–457; b) I. J. Bruno, J. C. Cole, P. R. Edgington, M. Kessler, C. F. Macrae, P. McCabe, J. Pearson, R. Taylor, *Acta Crystallogr. Sect. B* **2002**, *58*, 389–397.
[45] A. L. Spek, *J. Appl. Crystallogr.* **2003**, *36*, 7–13.
[46] M. J. Frisch, G. W. Trucks, H. B. Schlegel, G. E. Scuseria, M. A. Robb, J. R. Cheeseman, G. Scalmani, V. Barone, G. A. Petersson, H. Nakatsuji, X. Li, M. Caricato, A. V. Marenich, J. Bloino, B. G. Janesko, R. Gomperts, B. Mennucci, H. P. Hratchian, J. V. Ortiz, A. F. Izmaylov, J. L. Sonnenberg, Williams, F. Ding, F. Lipparini, F. Egidi, J. Goings, B. Peng, A. Petrone, T. Henderson, D. Ranasinghe, V. G. Zakrzewski, J. Gao, N. Rega, G. Zheng, W. Liang, M. Hada, M. Ehara, K. Toyota, R. Fukuda, J. Hasegawa, M. Ishida, T. Nakajima, Y. Honda, O. Kitao, H. Nakai, T. Vreven, K. Throssell, J. A. Montgomery Jr., J. E. Peralta, F. Ogliaro, M. J. Bearpark, J. J. Heyd, E. N. Brothers, K. N. Kudin, V. N. Staroverov, T. A. Keith, R. Kobayashi, J. Normand, K. Raghavachari, A. P. Rendell, J. C. Burant, S. S. Iyengar, J. Tomasi, M. Cossi, J. M. Millam, M. Klene, C. Adamo, R. Cammi, J. W. Ochterski, R. L. Martin, K. Morokuma, O. Farkas, J. B. Foresman, D. J. Fox, Gaussian 16, Revision B.01, Gaussian, Inc., *Wallingford*, CT **2016**.
[47] P. C. Hariharan, J. A. Pople, *Theor. Chim. Acta* **1973**, *28*, 213–222.
[48] a) C. Adamo, V. Barone, *J. Chem. Phys.* **1999**, *110*, 6158–6170; b) J. P. Perdew, K. Burke, M. Ernzerhof, *Phys. Rev. Lett.* **1996**, *77*, 3865–3868.

[49] a) W. Küchle, M. Dolg, H. Stoll, H. Preuss, *J. Chem. Phys.* **1994**, *100*, 7535–7542; b) M. Dolg, H. Stoll, H. Preuss, *J. Chem. Phys.* **1989**, *90*, 1730–1734.
[50] D. Andrae, U. Huermann, M. Dolg, H. Stoll, H. Preu, *Theor. Chim. Acta* **1990**, *77*, 123–141.
[51] a) G. Scalmani, M. J. Frisch, *J. Chem. Phys.* **2010**, *132*, 114110; b) M. Cossi, N. Rega, G. Scalmani, V. Barone, *J. Comput. Chem.* **2003**, *24*, 669–681; c) B. Mennucci, J. Tomasi, *J. Chem. Phys.* **1997**, *106*, 5151–5158; d) E. Cancès, B. Mennucci, J. Tomasi, *J. Chem. Phys.* **1997**, *107*, 3032–3041.
[52] N. M. O'Boyle, A. L. Tenderholt, K. M. Langner, *J. Comput. Chem.* **2008**, *29*, 839–845.
[53] X. Peng, T. E. Wilson, A. P. Alivisatos, P. G. Schultz, *Angew. Chem. Int. Ed.* **1997**, *36*, 145–147; *Angew. Chem.* **1997**, *109*, 113–115.

Manuscript received: June 14, 2022
Revised manuscript received: July 14, 2022
Accepted manuscript online: August 4, 2022

